

國立交通大學

電機與控制工程學系

碩士論文

時間延遲效應下遠端操控機器人系統之雙向



Bilateral Control of Internet-Based  
Telerobotic System under Time Delay

研究生：李國鋒

指導教授：楊谷洋 博士

中華民國九十三年七月

# 時間延遲效應下遠端操控機器人系統之雙向 控制

Bilateral Control of Internet-Based  
Telerobotic System under Time Delay

研究生：李國鋒

Student：Kuo-Feng Li

指導教授：楊谷洋

Advisor：Kuu-Young Young



碩士論文

A Thesis

Submitted to Department of Electrical and Control Engineering

College of Electrical Engineering and Computer Science

National Chiao Tung University

in partial Fulfillment of the Requirements

for the Degree of

Master

in

Computer and Information Science

July 2004

Hsinchu, Taiwan, Republic of China

中華民國九十三年 七月

# 時間延遲效應下遠端操控機器人系統之雙向控制

研究生： 李國鋒

指導教授： 楊谷洋教授

國立交通大學電機與控制工程學系

## 摘要

由於電腦網路使用的普遍性與方便性，網路連結遠端操控機器人系統成為一項熱門且持續在發展的研究領域。對一個網路連結遠端操控機器人系統而言，經由網路連結所造成的變動時間延遲對系統性能的影響也一直是這個領域經常討論的。當我們經由雙向的網路連結遠端操控機器人系統執行順應性工作時，可能會發生近端和遠端不同步以及系統不穩定的現象，而且，延遲過後的遠端資訊，可能讓操縱者會對遠端做出錯誤或不適當的命令，造成遠端機構的損壞；除了穩定性和同步性之外，時間延遲也可能降低系統的透明性。在此論文中，我們提出雙向控制策略來維持系統的穩定性，另外，由於同步性問題的難以解決，所以我們利用近端的虛擬實境遠端呈現技術來提供操縱者即時的位置預測及虛擬力反映，並且分析了整個系統架構的透明性。除此之外，我們還利用了事件驅動控制的方法建構一事件同步的遠端操控系統來和我們提出的系統架構做性能上的比較。最後經由模擬和實驗來驗證我們提出的控制策略之可行性及有效性。

# Bilateral Control of Internet-Based Telerobotic System under Time Delay

Student: Kuo-Feng Li

Advisor: Dr. Kuu-Young Young

Department of Electrical and Control Engineering  
National Chiao Tung University

## Abstract

Along with the prevalence and convenience of the computer network, the Internet-based telerobotic system becomes much more popular and has been continuously improved. In this research area, the influence of inherent varying time delay in the network on system performance has been intensively discussed. Especially, when a compliance task is executed using the bilateral internet-based telerobotic system, the time delay may invoke asynchronous and unstable phenomena evidently. In addition to stability and synchronicity, time delay may also degrade system transparency. In this thesis, we propose new bilateral control strategies to maintain system stability. And, because it is difficult to achieve system synchronicity in the presence of varying time delay, the VR-predictive display technique is used to furnish the predicted position and virtual contact force at the local site in a real-time manner. Besides, we also analyze the transparency of the proposed system. For comparison, an event-based teleoperation system that can achieve event-synchronicity is developed. Simulations and experiments are performed to verify the feasibility and the effectiveness of the proposed scheme.

# Acknowledgements

首先要感謝的是我的指導教授---楊谷洋博士，在這兩年的研究期間，承蒙老師耐心的指導，尤其是最後論文的寫作期間，老師細心的批改以及校閱，讓學生獲益良多並且順利完成我的碩士論文，同時也感謝林錫寬教授，宋開泰教授及蘇順豐教授於口試時給予學生論文上的指導與建議。感謝彬原、如駿、高平等實驗室同學及彥慶、福偉、柏駿、洺樞、建亨、明杰等學弟在課業上及生活上的幫助，最後我要感謝我的家人，因為你們在背後給我的支持和關懷，使我能夠順利完成學業，謝謝你們！



# Contents

<b>Chinese Abstract</b>	I
<b>English Abstract</b>	II
<b>Acknowledgements</b>	III
<b>Contents</b>	IV
<b>List of Figures</b>	VI
<b>1. Introduction</b> .....	1
<b>2. Proposed Bilateral Telerobotic system</b> .....	7
2.1 Original and modified control schemes.....	8
2.2 Major modules in the scheme.....	10
2.3 Model definitions and signal flow formulation.....	12
<b>3. Proposed control strategies</b> .....	15
3.1 Impedance controller.....	16
3.2 Sliding-mode impedance controller.....	17
3.3 Stability analysis.....	21
3.4 Transparency.....	23

3.5 Synchronicity.....	25
3.6 Event-based teleoperation system.....	26
3.6.1 Event-based control for teleoperation system.....	27
<b>4. Simulations.....</b>	<b>32</b>
4.1 Matlab simulation.....	33
4.2 VR-based predictive display.....	39
4.3 Tranparency.....	41
4.4 Event-based teleoperation system.....	44
<b>5. Experiments.....</b>	<b>48</b>
<b>6. Conclusion and Future Work.....</b>	<b>59</b>
6.1 Future work.....	60
<b>Bibliography.....</b>	<b>61</b>



# List of Figures

Fig. 1.1 A typical telerobotic system.....	2
Fig. 2.1 Block diagram of the proposed bilateral telerobotic system.....	8
Fig. 2.2 The original and modified control schemes.....	9
Fig. 2.3 Conceptual diagram of the proposed Internet-based bilateral telerobotic system.....	11
Fig. 2.4 Dynamic models for the one-DOF master-slave system.....	12
Fig. 2.5 Signal flows in the proposed bilateral telerobotic system.....	14
Fig. 3.1 Block diagram of the proposed bilateral telerobotic control scheme.....	16
Fig. 3.2 A two-port representation of a telerobotic system.....	24
Fig. 3.3 A diagram of action reference for path-based control.....	27
Fig. 3.4 System architecture of the event-based teleoperation system.....	28
Fig. 3.5 Flowchart of the algorithm for the event-based teleoperation system.....	29
Fig. 4.1 Position and force responses of the proposed scheme without time delay....	34
Fig. 4.2 Position and force responses of the proposed scheme under constant time delay.....	35



Fig 4.3 Position and force responses of the proposed scheme under varying time delay.....	37
Fig 4.4 Position and force responses of the proposed scheme under larger varying time delay.....	38
Fig. 4.5 Position and force responses of the master and slave using the VR-based predictive display.....	40
Fig. 4.6 Magnitude and phase responses of the impedance transfer function when contact with hard wall.....	42
Fig. 4.7 Magnitude and phase responses of the impedance transfer function when contact with soft wall.....	43
Fig. 4.8 Position and force responses of the event-based teleoperation system in event domain.....	46
Fig. 4.9 Position and force responses of the event-based teleoperation system in time domain.....	47
Fig. 5.1 The profile of round-trip delay that each master command encountered between two computers in NCTU.....	49
Fig. 5.2 Internet experimental results in performing the compliance task between two computers in NCTU.....	50
Fig. 5.3 The profile of round-trip delay that each master command encountered between two computers in NCTU and NCKU.....	51

Fig. 5.4 Internet experimental results in performing the compliance task between two computers in NCTU and NCKU.....52

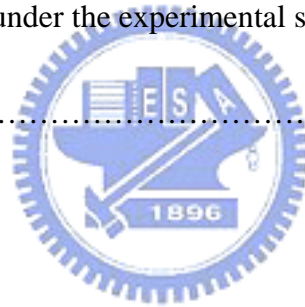
Fig. 5.5 The profile of round-trip delay that each master command encountered between two computers in Taiwan and USA.....53

Fig. 5.6 Internet experimental results in performing the compliance task between two computers in Taiwan and USA.....54

Fig. 5.7 The laparoscopic impulse engine.....56

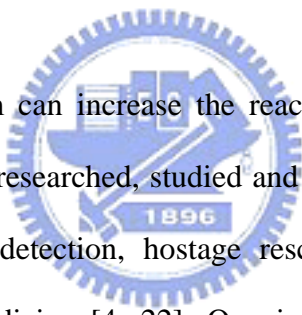
Fig. 5.8 The experimental setup.....57

Fig. 5.9 Experimental results under the experimental setup as described in Fig. 5.8 .....58



# Chapter 1

## Introduction



The teleoperation system can increase the reachability and safety of humans. Thus, it has been extensively researched, studied and applied in many fields, such as space exploration, undersea detection, hostage rescue operation, maintenance of nuclear facilities, and telemedicine [4, 22]. One important factor in a telerobotic system is telepresence. Telepresence stands for the transfer of human senses to remote location by feeding back sensory information from the remote environment. In early telerobotic systems, usually only visual information is fed back to the operator. However, the information is not sufficient when the tasks involve interaction with the remote environment. To achieve the realism and efficiency in teleoperation, the force information between the slave manipulator and remote environment may also need to be transmitted to the operator. This would closely couple the operator with the remote environment and thus gives a more realistic feeling of presence.

Fig. 1.1 shows a typical telerobotic system, which consists mainly of a master

mechanism (here a force reflection joystick) and a slave manipulator. The human operator manipulates the joystick to generate position, velocity, or force commands, which consequently move the remote slave manipulator to execute tasks via the communication channel. Conversely, the visual and force information are transmitted back to the master site for the operator to sense the remote environment.

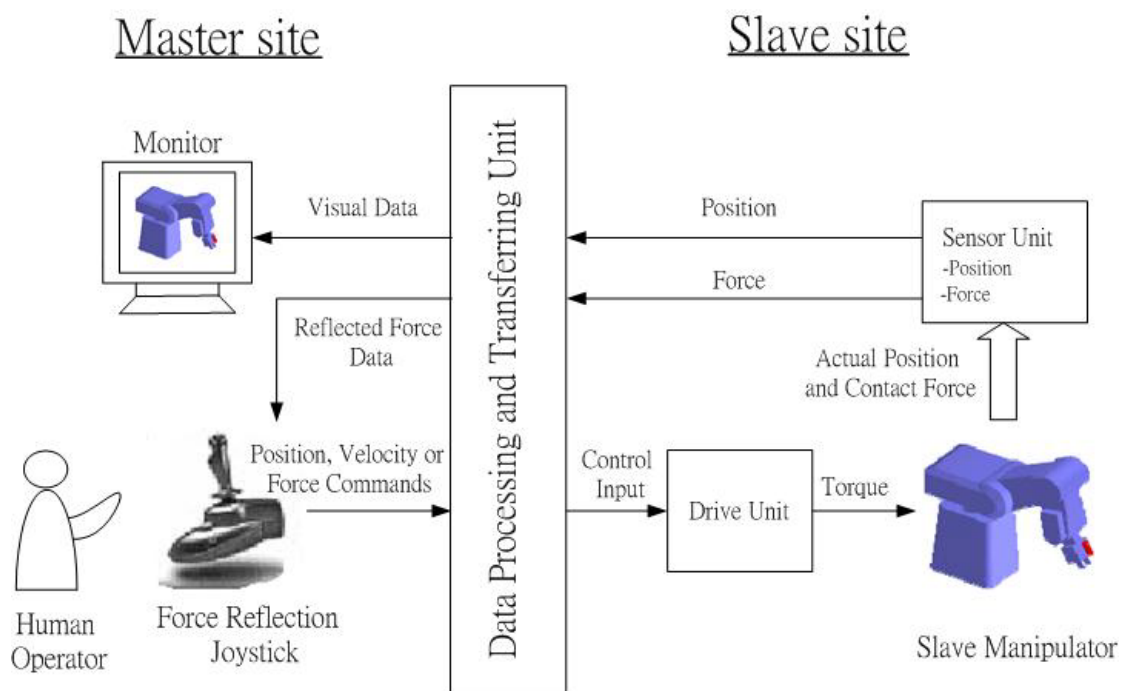


Fig. 1.1 A typical telerobotic system.

Recently, more and more computer networks are used as the communication channels of bilateral teleoperation systems. It is because computer networks, such as Internet, are easier to be implemented and much more flexible than the dedicated private communication channels. When we use the Internet as a data transmission medium for telerobotic tasks, we need to consider the influence of time delay [1]. For a teleoperation system, several safety and performance specifications have to be met. Among them, stability, transparency, and synchronicity are the main focuses. Ensuring these features in teleoperation systems, specifically those Internet-based

systems, is very challenging. The difficulties are mainly invoked by time delay in such networks. Even a small constant time delay can make bilateral systems unstable and consequently degrade system performance [2].

Several control methods have been proposed to tackle the instability problem invoked by time delay. Oboe and Fiorini presented a computer environment for designing, simulating, and testing control algorithms for Internet-based telerobotic systems. The delay parameters are identified by probing the network. These parameters are then used in the design of a controller [19]. Anderson and Spong guaranteed the communication block to be a passive element by using scattering transformation to overcome the instability caused by time delay [3]. This method can only be applied to the communication block with constant time delay. Kosuge et al. used “virtual time delay” to keep the time delay constant when using scattering transformation to tackle varying time delay [13-14]. This method stores the commands received from the master site in a buffer and send them to the slave for task execution periodically. Thus, the delay can be regulated to a constant value. Niemeyer and Slotine showed that the stability of bilateral telerobotic systems in the presence of irregular time delay can be preserved through the use of wave variable filters [18]. Yokokohji et al. proposed a compensator based on wave variables to alleviate the performance degradation due to varying time delays [30-31]. Park and Cho proposed a sliding mode control scheme to achieve system stability under varying time delays [20]. Prokopiou et al. proposed a master state prediction method [23]. This method uses the prediction of master state (position and force), and incorporates it in a stable force-feedback control scheme.

Although those methods discussed above can provide stability, they did not

ensure synchronicity and transparency. Real-time teleoperation system is difficult to achieve due to the inherent time delay in the computer networks. One solution is to develop faster and more efficient network communication protocols to provide better real-time data transmission capability. It is certainly not an easy task. Some researchers proposed using event-based control to deal with the time delay problem [29,28,6-9]. Xi et al. proposed a method for action synchronization and control of telerobotic systems based on the event-based control algorithm [29,28]. Event-based control is basically a non-time-based control which uses event instead of time as action reference. Since the system status is driven by event instead of time, the system becomes immune to delay. The system synchronicity achieved is according to event instead of time reference, and it is also called event-synchronization. In the time domain, it seems that the slave manipulator has to wait until the control input of next event arrives. Thus, the human operator needs to “work and wait”, which is unnatural and ineffective in manipulation. The event-based teleoperation systems can only achieve event-synchronization, but still not time-synchronization. In addition, the slave manipulator exhibits a non-smooth motion, and the measured contact force for each event between the slave and the environment is distorted under large time delay.

As for transparency, it means that when the operator manipulates the master, he (she) may have felt like manipulating the slave directly [33]. In a teleoperation system, the human operator interacts with the environment without direct contact between them. Ideally, such a system would completely preserve the “feel” of the environment with which the operator interacts. In reality, however, the system cannot achieve it due to many factors, like delay effect, system architecture, bilateral control strategies, etc. It is not that straightforward to quantify the degree of “feel” from the remote site to the operator through the teleoperation system. Salcudean et al. quantified transparency

as the match between the mechanical impedance of the environment experienced by the slave and that transmitted to the human operator [33]. Salcudean and Zadd analyzed the transparency of a bilateral telerobotic system with transmission time delay and achieved transparent bilateral control in the presence of time delay [32]. Elhajjetal et al. also applied event-transparency for the event-based bilateral telerobotic system and verified it via experiments [8]. Related researches for transparency can also be found in [15,27].

Previously in our laboratory, a bilateral telerobotic control scheme based on the sliding-mode control together with compliance control has been proposed to achieve system stability during task execution in the presence of varying time delay. And, VR-based predictive display technique has been used to furnish the human operator with the predicted visual and force information of the remote system. In this thesis, we modify previous approach and propose a new scheme based on sliding-mode-impedance control to achieve system stability. The VR-based predictive display technique is still preserved with improvement to provide real-time predicted position and virtual contact force from the VR environment at the master site. With the predicted position and force response from remote environment, the human operator can interact with the virtual robot constructed in VR environment with much less influence from time delay. Furthermore, we also analyze system transparency under the proposed scheme. Based on the concept of event-based control, which claimed that it can eliminate the asynchronous phenomenon, we develop an event-based bilateral control scheme in this thesis for the purpose of performance comparison. Finally, we perform Internet experiments within NCTU, between NCTU and NCKU, and between Taiwan and U.S.A to evaluate system performance.

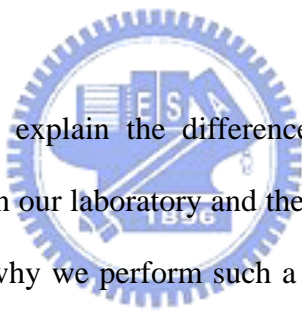
The rest of the thesis is organized as follows. Chapter 2 describes the proposed scheme. In Chapter 3, the proposed bilateral control strategies and issues on the stability, synchronicity and transparency are discussed. For performance comparison, an event-based control scheme is also built in Chapter 3. Simulations and experiments are described in Chapters 4 and 5, respectively. Chapter 6 gives the conclusion and some future works.





## Chapter 2

# Proposed Bilateral Telerobotic System



In this chapter, we first explain the difference between the original control scheme in the previous work in our laboratory and the proposed scheme in this thesis, including the motivations of why we perform such a modification. We then describe the major modules in the proposed bilateral telerobotic system, shown in Fig. 2.1, which consists of mainly the sliding-mode-impedance controller at the remote site to track the master commands and maintain force stability, impedance controller at the local site to reduce too large reflected force on the master, and VR-based predictive display at the local site to provide real-time predicted position and virtual force information for the master. Finally, before elaborating the control law design and system analysis, we give the model definitions and signal flow formulation.

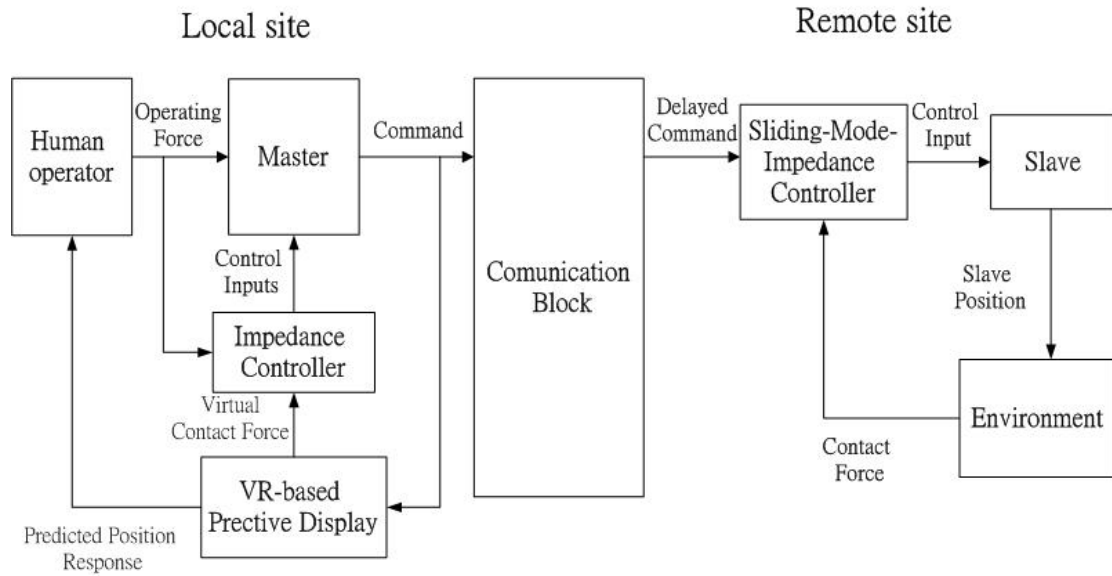
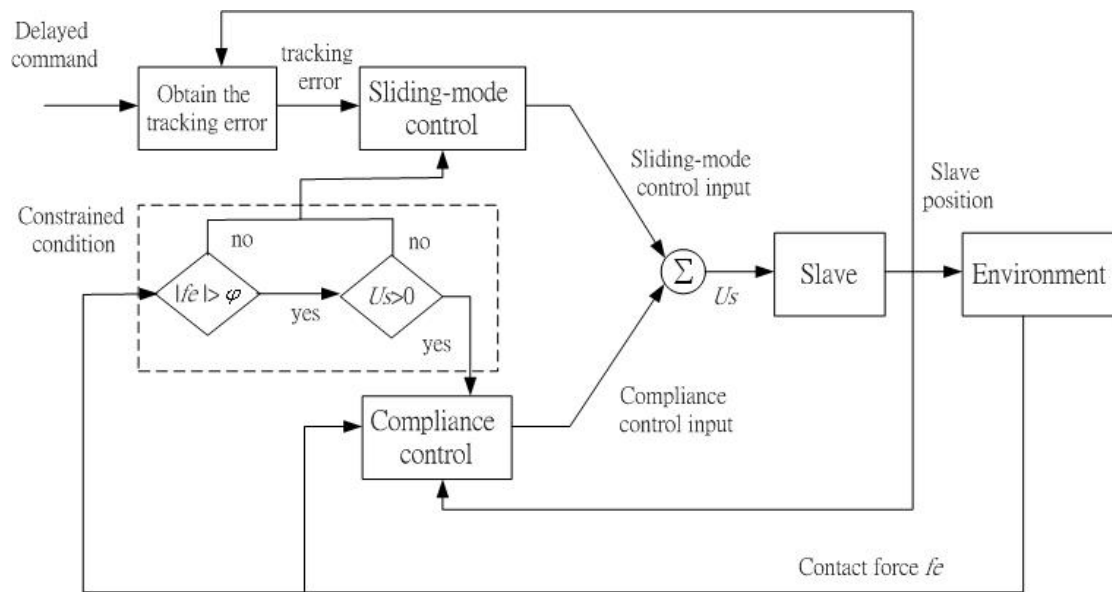


Fig. 2.1 Block diagram of the proposed bilateral telerobotic system.

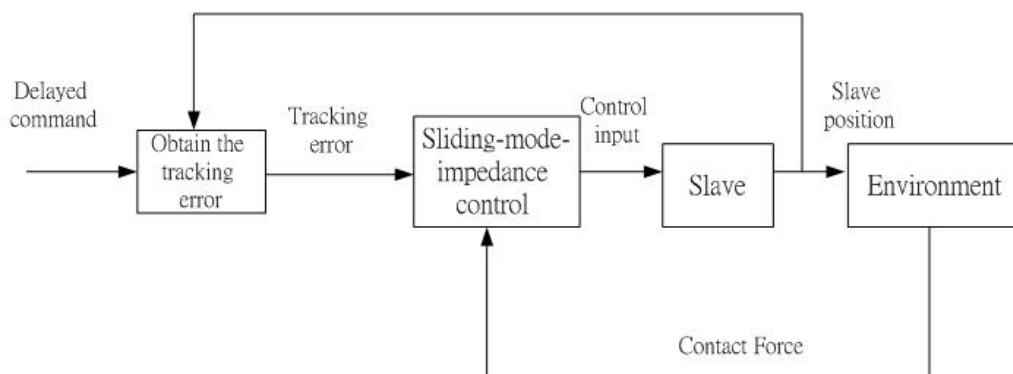
## 2.1 Original and modified control schemes

Fig. 2.2(a)-(b) show the original and modified control schemes, respectively. In the original scheme shown in Fig. 2.2(a), the sliding-mode controller together with compliance controller are used to achieve system stability. In unconstrained motion, the sliding-mode controller executes the path tracking; in constrained motion, the compliance controller takes charges in executing the compliance task. The control input changes depending on the condition of whether the slave manipulator contacts with the environment. The switch may make the system unstable [24], and make it not easy for system analysis and performance evaluation. In addition, it increases the implementation complexity. We thus propose the sliding-mode-impedance control scheme, as shown in Fig. 2.2(b), for replacement. In this scheme, we introduce a target impedance specified for the slave. With proper design of the control law, we can “latch” the slave impedance behavior on the desired target impedance in the presence of varying time delay. Hence, the sliding-mode-impedance controller has the

capability to execute path tracking and to maintain a stable contact force simultaneously. With this simplified control scheme, as shown in Fig.2.2 (b), it makes the following system analysis and performance evaluation more meaningful. Detailed descriptions of the control law design will be given in next chapter.



(a) Original scheme



(b) Modified scheme

Fig. 2.2 The original and modified control schemes: (a) the original scheme, and (b) the proposed scheme.

## 2.2 Major modules in the scheme

Except the sliding-mode-impedance controller to be described in Chapter 3, the other major modules in the proposed scheme are discussed below.

### A. Impedance controller

To avoid the master mechanism damaged by too large reflected force, we also adopt an impedance controller at the local site, like the previous work in our laboratory. With the impedance controller, the relation between the operating force, master position, and the contact force from the slave can be regulated following a desired impedance characteristic. The reduced force reflection can thus be scaled down to a safe range, such that the operator can bear.

### B. Internet communication protocol

For a bilateral telerobotic system, the control signals on the master are transmitted to the slave and the feedback forces from the slave sent back to the master via the communication medium. Fig. 2.3 shows a conceptual diagram of the proposed Internet-based bilateral telerobotic system. In the Internet communication, TCP (Transmission Communication Protocol) and UDP (User Datagram Protocol) are used as the standard communication protocol. However, the loss of data packets may occur and the orders of the sending data packets be changed when transmitted with UDP. Thus, we adopt the TCP as the Internet communication protocol to prevent abrupt data changes due to its error recovery and reordering capability.

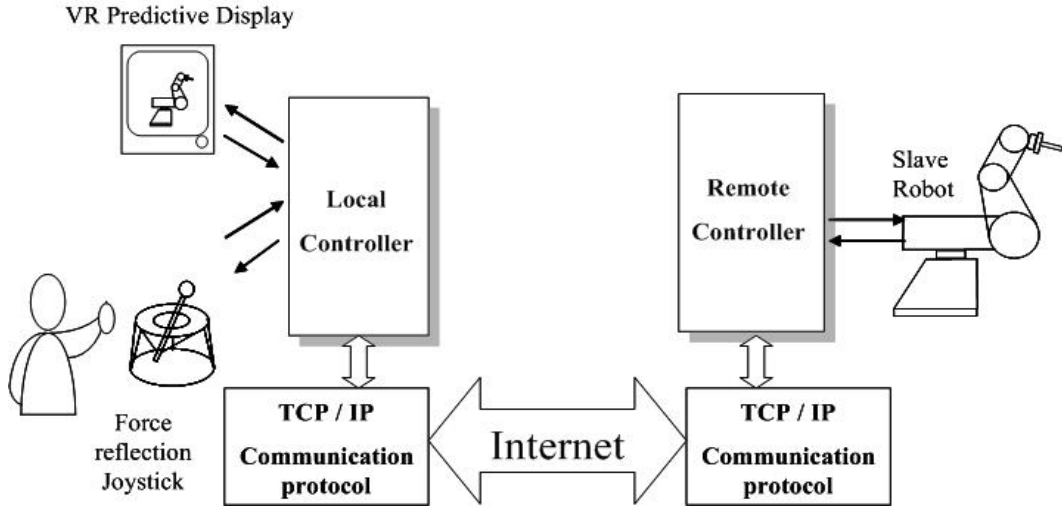


Fig. 2.3 Conceptual diagram of the proposed Internet-based bilateral telerobotic system.

### C. VR-based predictive display

In Fig. 2.1, VR (Virtual Reality) predictive display is used to provide real-time predicted visual (position) information and virtual contact force at the master site. The availability of the visual signal together with force reflection in the telerobotic system can improve efficiency, maneuverability, and safety. When the human operator, via the virtual robot, interacts with the virtual objects, the predicted contact force of the between the slave and environment will be generated according to the estimated stiffness of the remote object. When only the stiffness of the object is considered, the predicted force is defined as

$$F_r = K_o (x - x_c) \quad (2.1)$$

where  $F_r$  stands for the generated reflected force,  $x_c$  the location of the contact point,  $K_o$  the estimated stiffness of the object, and  $x$  the position of the virtual robot. The least-square linear regression method can be used for estimating stiffness of remote object through processing a series of measured position and force data.

With the stiffness approximating the real one, the VR simulator will be able to provide accurate virtual contact force.

## 2.3 Model definitions and signal flow formulation

Before the discussion of the proposed control strategies, we first describe the models of the master and slave systems. Refer to Fig. 2.4, the dynamics of the single DOF master/slave system are modeled as a mass-damper system:

$$\mathbf{M}_m \ddot{x}_m(t) + \mathbf{B}_m \dot{x}_m(t) = u_m(t) + f_h(t) \quad (2.2)$$

$$\mathbf{M}_s \ddot{x}_s(t) + \mathbf{B}_s \dot{x}_s(t) = u_s(t) - f_e(t) \quad (2.3)$$

where  $x$  and  $u$  denote position and control input torque, respectively,  $M$  and  $B$  mass and viscous coefficients with subscript 'm' and 's' denoting the master and slave, respectively,  $f_h$  the force applied on the master by the human operator, and  $f_e$  the force exerted on the slave by its environment.

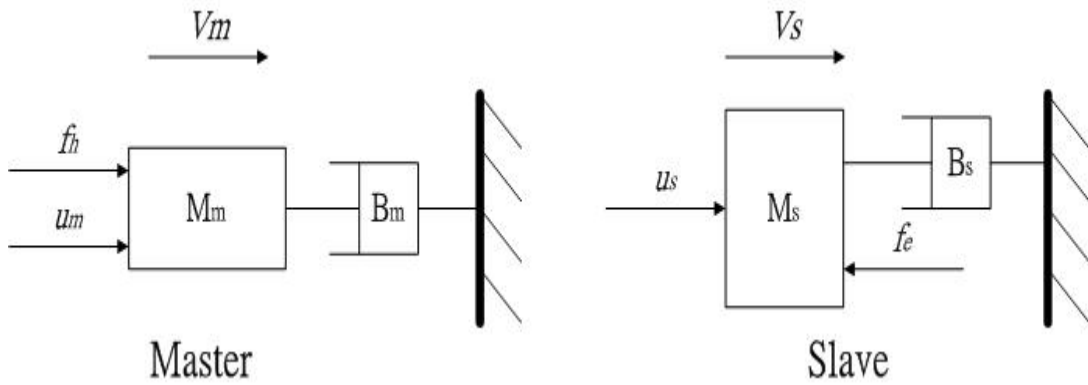


Fig. 2.4 Dynamic models for the one-DOF master-slave system.

The major signal flows in the proposed bilateral telerobotic system are as shown in Fig. 2.5, where  $x_{md}$ ,  $v_{md}$ , and  $f_{hd}$  are the position, velocity, and operating force, respectively, transmitted from the master to the slave, and  $f_{ed}$  is the feedback force, transmitted from the slave to the master. We formulate the delayed signals as

$$x_{md}(t) = x_m(t - T_1(t)) \quad (2.4)$$

$$v_{md}(t) = v_m(t - T_1(t)) \quad (2.5)$$

$$f_{hd}(t) = f_h(t - T_1(t)) \quad (2.6)$$

$$f_{ed}(t) = f_e(t - T_2(t)) \quad (2.7)$$

where  $T_1(t)$  and  $T_2(t)$  are the transmission time delays from the master to slave and from the slave to master, respectively. Note that these delays vary along with time  $t$ , and also the direction as well as the computer network condition [16].

Because the working condition of the master is different from that of the slave, the delayed signals out of the communication block, described in Eqs.(2.4)-(2.7), may need to be scaled up or down. With the scaling factors, the relationship between the master and the slave on position and force are formulated as:

$$x_s(t) = k_p x_{md}(t) \quad (2.8)$$

$$f_m(t) = k_f f_{ed}(t) \quad (2.9)$$

where  $x_s$  denotes the slave position command,  $f_m$  is the applied force on the master, and  $k_p$  and  $k_f$  the constant position and force scaling factor, respectively.

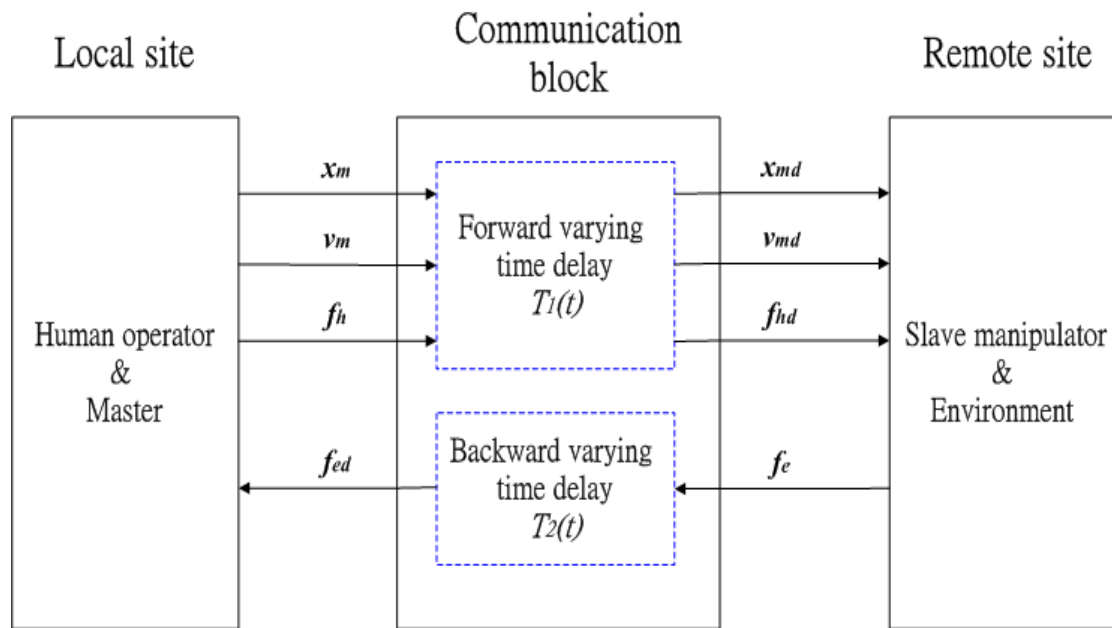


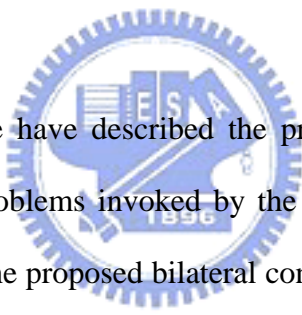
Fig. 2.5 Signal flows in the proposed bilateral telerobotic system.





## Chapter 3

# Proposed Control Strategies



In Chapters 1 and 2, we have described the proposed Internet-based bilateral telerobotic system and the problems invoked by the time delay. In this chapter, we give detailed descriptions of the proposed bilateral control strategies. We then analyze the stability and transparency of the system and comment on the synchronicity issue. Because the inherent varying time delay problem in the computer networks, some researchers propose the event-based control method to construct an event-synchronized teleoperation system instead of time to eliminate the asynchronous phenomenon in the communication links. Due to its popularity and effectiveness, we also develop an event-based teleoperation system for performance comparison.

Fig. 3.1 shows the block diagram of the proposed bilateral telerobotic control scheme, including the impedance controller for the master to reduce the reflected force imposed on the joystick and the sliding-mode-impedance controller for the slave to deal with command tracking and maintain force stability. In Fig. 3.1,  $x_m(t)$ ,  $v_m(t)$

denote the master position, velocity, respectively,  $x_s(t)$ , the slave position,  $u_m(t)$ , the master site control input,  $u_s(t)$ , the slave site control input,  $f_h(t)$ , the operating force, and  $f_e(t)$ , the force exerted on the slave by its environment.

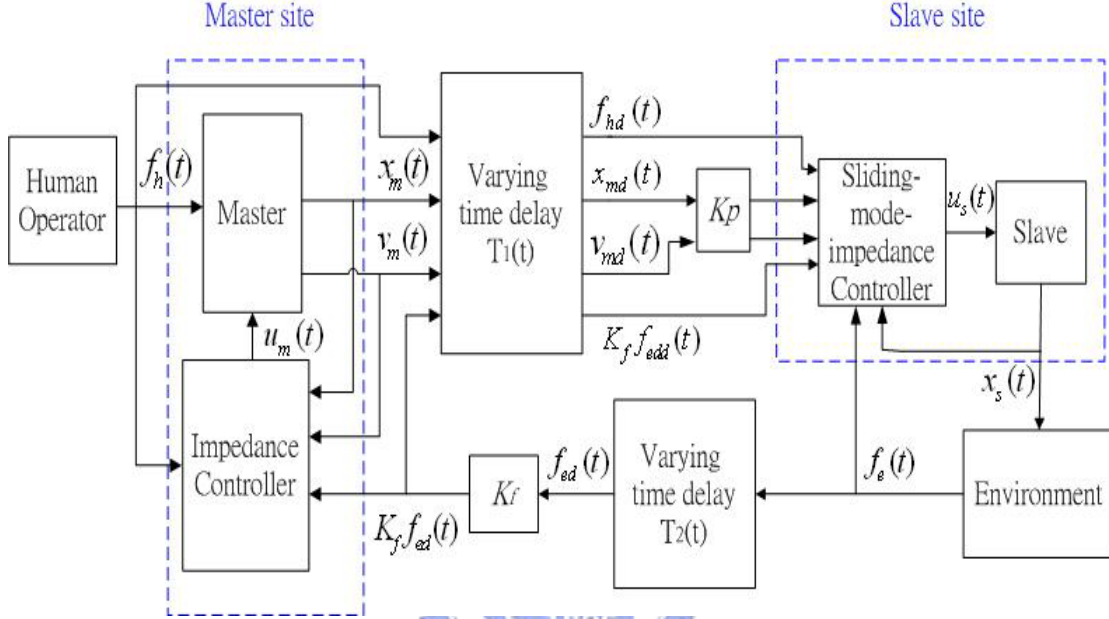


Fig. 3.1 Block diagram of the proposed bilateral telerobotic control scheme.

### 3.1 Impedance controller

In the bilateral telerobotic system, the master must reflect to the human operator the contact force between the slave manipulator and the environment. With the impedance controller, the relation between the operating force, master position, and the contact force from the slave can be regulated to a desired impedance characteristic, and, the impact force reflected on the human operator can be scaled down to a safe range, preventing the master from damage by too large contact force. For this, the desired impedance characteristic is specified for the master as

$$M\ddot{x}_m(t) + B\dot{x}_m(t) + Kx_m(t) = f_h(t) - k_f f_{ed}(t) \quad (3.1)$$

where  $M$ ,  $B$ , and  $K$  denote the desired inertia, damping, and stiffness, respectively,  $x_m(t)$ ,  $\dot{x}_m(t)$ , and  $\ddot{x}_m(t)$  the master position, velocity, acceleration, respectively,  $k_f$ ,  $k_p$  the force, position scaling factor, respectively,  $f_{ed}(t)$  the delayed force signal from the slave, and  $f_h(t)$  the force applied on the master by the human operator. By combining the dynamics of the master system, described in Eq.(2.2), with its desired impedance characteristic, described in Eq.(3.1), the control input for the master  $u_m(t)$  can be obtained as

$$u_m(t) = (B_m - \frac{M_m B}{M})v_m(t) + (\frac{M_m}{M} - 1)f_h(t) - \frac{M_m}{M}[k_f f_{ed}(t) + Kx_m(t)] \quad (3.2)$$



### 3.2 Sliding-mode-impedance controller

Sliding-mode control is recognized as a robust control method in the presence of modeling uncertainties and external disturbances [34]. In our previous works, the sliding-mode controller was used for path tracking in unconstrained motion under varying time delay. And, the compliance controller was used for force stability in constrained motion. With two controllers, the system was complicated and control inputs might switch, thus susceptible to system instability.

Therefore, we propose using the sliding-mode-impedance controller. Impedance control is a well known position/force control method which specifies a relation between external force and the slave position. Together with the sliding-mode control, the sliding-mode-impedance controller utilizes the robust property of the sliding-mode control against uncertainties, such as external disturbance and varying

time delay. In this controller, the sliding surface includes a desired impedance characteristic of the slave, and the slave exhibits its desired impedance behavior when the controller satisfies the sliding condition. The control law design is described as follows.

A target impedance characteristic for the slave to perform a compliance task under varying time delay is specified as

$$\bar{m}_s \tilde{x}_{sd}''(t) + \bar{b}_s \tilde{x}_{sd}'(t) + \bar{k}_s \tilde{x}_{sd}(t) = -f_e(t) \quad (3.3)$$

where  $\bar{m}_s$ ,  $\bar{b}_s$  and  $\bar{k}_s$  are the desired inertia, damping coefficient, and stiffness, respectively, and

$$\tilde{x}_{sd}(t) = x_s(t) - k_p x_{md}(t) \quad (3.4)$$

$$\tilde{x}_{sd}'(t) = \dot{x}_s(t) - k_p \dot{x}_{md}(t) \quad (3.5)$$

$$\tilde{x}_{sd}''(t) = \ddot{x}_s(t) - k_p \ddot{x}_{md}(t) \quad (3.6)$$

As mentioned before, the purpose of this controller is to force the slave's impedance behavior toward the target impedance. Thus, the impedance error,  $I_e(t)$ , is defined as

$$I_e(t) = \bar{m}_s \tilde{x}_{sd}''(t) + \bar{b}_s \tilde{x}_{sd}'(t) + \bar{k}_s \tilde{x}_{sd}(t) + f_e(t) \quad (3.7)$$

Next, we define the sliding function as

$$\begin{aligned}
s(t) &= \frac{1}{\bar{m}_s} \int_0^t I_e(\tau) d\tau \\
&= \dot{x}_s(t) + \frac{\bar{b}_s}{\bar{m}_s} x_s(t) + \frac{\bar{k}_s}{\bar{m}_s} \int_0^t x_s(\tau) d\tau - k_p \int_0^t \dot{x}_m(\tau - T_1(\tau)) d\tau \\
&\quad - \frac{1}{\bar{m}_s} \int_0^t [\bar{b}_s \dot{x}_m(\tau - T_1(\tau)) + \bar{k}_s x_m(\tau - T_1(\tau))] d\tau \\
&\quad + \frac{1}{\bar{m}_s} \int_0^t f_e(\tau) d\tau
\end{aligned} \tag{3.8}$$

Therefore, it is clear that when the sliding condition is satisfied, then the trajectory of  $s(t)$  will approach and slide on the sliding surface ( $s(t)=0$ ), which implies that  $I_e(t)$  will approach to zero, thus, the slave will exhibit the desired impedance behavior. Then, by time shifting  $T_1(t)$ , we can derive the delayed master acceleration signal from Eq.(3.1) as

$$\ddot{x}_{md}(t) = \frac{f_{hd}(t) - k_f f_{edd}(t) - \mathbf{B}v_{md}(t) + \mathbf{K}x_{md}(t)}{\mathbf{M}} \tag{3.9}$$

The delayed external force signal  $f_{edd}(t) = f_e(t - T_1(t) - T_2(t))$  can be obtained by sending the external force  $f_{ed}(t) = f_e(t - T_2(t))$  from the master to the slave as shown in Fig. 3.1. Substituting Eq.(3.9) into Eq.(3.8), we can obtain

$$\begin{aligned}
s(t) &= \dot{x}_s(t) + \frac{\bar{b}_s}{\bar{m}_s} x_s(t) + \frac{\bar{k}_s}{\bar{m}_s} \int_0^t x_s(\tau) d\tau + k_p \left( \frac{\mathbf{B}}{\mathbf{M}} - \frac{\bar{b}_s}{\bar{m}_s} \right) \int_0^t \dot{x}_m(\tau - T_1(\tau)) d\tau \\
&\quad + k_p \left( \frac{\mathbf{K}}{\mathbf{M}} - \frac{\bar{k}_s}{\bar{m}_s} \right) \int_0^t x_m(\tau - T_1(\tau)) d\tau - \int_0^t \left[ \frac{k_p}{\mathbf{M}} \{ f_h(\tau - T_1(\tau)) \right. \\
&\quad \left. - k_f f_e(\tau - T_1(\tau) - T_2(\tau)) \} - \frac{1}{\bar{m}_s} f_e(\tau) \right] d\tau
\end{aligned} \tag{3.10}$$

By differentiating Eq.(3.10) with respect to time  $t$ , we can obtain the first order differential equation of  $s(t)$  as

$$\begin{aligned}
\dot{s}(t) &= \ddot{x}_s(t) + \frac{\bar{b}_s}{\bar{m}_s} \dot{x}_s(t) + \frac{\bar{k}_s}{\bar{m}_s} x_s(t) + k_p \left( \frac{\mathbf{B}}{\mathbf{M}} - \frac{\bar{b}_s}{\bar{m}_s} \right) \dot{x}_{md}(t) \\
&\quad + k_p \left( \frac{\mathbf{K}}{\mathbf{M}} - \frac{\bar{k}_s}{\bar{m}_s} \right) x_{md}(t) - \left[ \frac{k_p}{\mathbf{M}} \{ f_{hd}(t) - k_f f_{edd}(t) \} - \frac{1}{\bar{m}_s} f_{ed}(t) \right]
\end{aligned} \tag{3.11}$$

From the dynamics of the slave system described in Eq.(2.3), we can obtain the slave acceleration as

$$\ddot{x}_s(t) = \frac{u_s(t) - f_e(t) - B_s \dot{x}_s(t)}{M_s} \quad (3.12)$$

Then, the replacement of  $\ddot{x}_s(t)$  in Eq.(3.11) by Eq.(3.12) gives the following result:

$$\begin{aligned} \dot{s}(t) = & \frac{u_s(t) - f_e(t) - B_s \dot{x}_s(t)}{M_s} + \frac{\bar{b}_s}{\bar{m}_s} \dot{x}_s(t) + \frac{\bar{k}_s}{\bar{m}_s} x_s(t) + k_p \left( \frac{B}{M} - \frac{\bar{b}_s}{\bar{m}_s} \right) \dot{x}_{md}(t) \\ & + k_p \left( \frac{K}{M} - \frac{\bar{k}_s}{\bar{m}_s} \right) x_{md}(t) - \left[ \frac{k_p}{M} \{ f_{hd}(t) - k_f f_{edd}(t) \} - \frac{1}{\bar{m}_s} f_{ed}(t) \right] \end{aligned} \quad (3.13)$$

The equivalent control [34] is obtained by using  $\dot{s} = s = 0$ . Thus, for solving the slave control law  $u_s(t)$ , we let  $\dot{s}(t)$  in Eq.(3.13) to be zero. By considering the uncertainties like the randomness of time delay, the sliding-mode-impedance control law for the slave can then be obtained as

$$\begin{aligned} u_s(t) = & -k_p \frac{M_s}{M} [B \dot{x}_{md}(t) + K x_{md}(t) - f_{hd}(t) + k_f f_{edd}(t)] - \frac{M_s}{\bar{m}_s} [\bar{b}_s \tilde{x}'_{sd}(t) \\ & + \bar{k}_s \tilde{x}_{sd}(t)] + B_s \dot{x}_s(t) + \left( 1 - \frac{M_s}{\bar{m}_s} \right) f_e(t) - k_g \cdot \text{Sat}\left(\frac{s(t)}{\varepsilon}\right) \end{aligned} \quad (3.14)$$

where  $k_g$  is a nonlinear gain,  $\varepsilon$  the boundary layer thickness, which is used for reducing the chattering of the control input, and  $\text{Sat}(\cdot)$  a saturation function defined as

$$\text{Sat}\left(\frac{s(t)}{\varepsilon}\right) = \begin{cases} 1 & s(t) > \varepsilon \\ \frac{s(t)}{\varepsilon} & |s(t)| \leq \varepsilon \\ -1 & s(t) < -\varepsilon \end{cases} \quad (3.15)$$

### 3.3 Stability analysis

The basic concept of sliding-mode control is to force the system states toward a sliding surface in the presence of modeling uncertainties and external disturbance. When the control input satisfies the approach and sliding condition of

$$s(t)\dot{s}(t) < -\sigma|s(t)| \quad (3.16)$$

where  $\sigma$  is the approaching rate and  $\sigma > 0$ , the system states will approach the sliding surface ( $s(t) = 0$ ) in a finite time. It has been shown in [34] that if the Lyapunov function is selected as

$$L = \frac{1}{2} s^T s \quad (3.17)$$

The sliding condition described in Eq.(3.16) will be satisfied when  $\dot{L} < 0$ . Obviously, in Eq.(3.17),  $L \geq 0$  and  $L = 0$ , only when  $s(t) = 0$ .

Because the sliding function is first order differentiable with respect to time, we can obtain the derivative of Eq.(3.17) as

$$\dot{L} = s(t)\dot{s}(t) \quad (3.18)$$

Then, the replacement of  $u_s(t)$  in Eq.(3.13) by Eq.(3.14) yields Eq.(3.19)

$$\dot{s}(t) = -\frac{k_g}{M_s} \text{sat}\left(\frac{s(t)}{\varepsilon}\right) \quad (3.19)$$

By substituting Eq.(3.19) into Eq.(3.18), it leads to

$$\dot{L} = s(t)\left[-\frac{k_g}{M_s} \text{sat}\left(\frac{s(t)}{\varepsilon}\right)\right] \quad (3.20)$$

In Eq.(3.20), it can be shown that  $\dot{L} < 0$  is satisfied with the designed slave input control law. Thus,  $L$  is really a Lyapunov function and gradually converge to zero with the proposed control input. Therefore,  $s(t)$  will also approach to zero in a finite time.

Next, we multiply both sides of Eq.(3.19) with  $s(t)$ , which leads to

$$\begin{aligned} s(t)\dot{s}(t) &= -\frac{k_g}{M_s} \text{sat}\left(\frac{s(t)}{\varepsilon}\right)s(t) \\ &= -\frac{K_g}{M_s} |s(t)| \end{aligned} \quad (3.21)$$

Then, by substituting Eq.(3.21) into Eq.(3.16), we can obtain

$$k_g > M_s \cdot \sigma \quad (3.22)$$

We found that the nonlinear gain  $k_g$  in Eq.(3.22) consists of only constant values, not the function of varying time delays,  $T_1(t)$  and  $T_2(t)$ . It means that  $k_g$  can be selected independently of the time delay and the scaling factors. Thus, with proper gain,  $k_g$ , the trajectory is kept in the region around the sliding surface. In this case, the slave exhibits the target impedance characteristic since  $I_e = \bar{m}_s \dot{s} \approx 0$ .





### 3.4 Transparency

In addition to stability, we also need to consider another important factor, transparency. Ideally, the teleoperation system would be completely transparent, so the ‘feel’ of remote environment at the slave can be faithfully preserved during task execution. In general, transparency can be quantified in terms of the match between the mechanical impedance of the environment encountered by the slave and that felt by the human operator.

In Fig. 3.2, the teleoperation system is modeled as a two-port network, where the operator-master interface is modeled as the master port and the slave-environment interface as the slave port. The relationship between *efforts* ( $f_h, f_e$ ) and *flows* ( $\dot{x}_m, \dot{x}_s$ ) can be described in terms of the so-called hybrid matrix obtained from the properly controlled master and slave behaviors described in Eqs. (3.1) and (3.3). Thus, the hybrid matrix for the teleoperation system and its parameters are formulated as

$$\begin{bmatrix} F_h(s) \\ V_s(s) \end{bmatrix} = \begin{bmatrix} h_{11} & h_{12} \\ h_{21} & h_{22} \end{bmatrix} \begin{bmatrix} V_m(s) \\ -F_e(s) \end{bmatrix} \quad (3.23)$$

where  $F_h(s)$ ,  $V_m(s)$ ,  $V_s(s)$ , and  $F_e(s)$  are the Laplace transforms of  $f_h(t)$ ,  $\dot{x}_m(t)$ ,  $\dot{x}_s(t)$ , and  $f_e(t)$ , respectively, and  $h$ -parameters as

$$h_{11} = Ms + B + \frac{K}{s} \quad (3.24)$$

$$h_{12} = -k_f \cdot e^{-T_2 s} \quad (3.25)$$

$$h_{21} = k_p \cdot e^{-T_1 s} \quad (3.26)$$

$$h_{22} = \frac{s}{\bar{m}_s s^2 + \bar{b}_s s + \bar{k}_s} \quad (3.27)$$

Refer to Fig. 3.2, the environmental impedance can be express as

$$Z_e = \frac{F_e(s)}{V_s(s)} \quad (3.28)$$

From above, we can express the transmitted impedance “felt” by the operator as

$$Z_t(s) = \frac{F_h(s)}{V_m(s)} = \frac{h_{11}(1+h_{22}Z_e) - h_{12}h_{21}Z_e}{1+h_{22}Z_e} \quad (3.29)$$

By investigating Eq.(3.29), we found the conditions for satisfying *completely transparency* ( $Z_t = Z_e$ ) to be

$$\begin{aligned} h_{11} &= h_{22} = 0 \\ h_{12}h_{21} &= -1 \end{aligned} \quad (3.30)$$

In practice, completely transparent teleoperation is not possible. There are many factors that influence transparency during teleoperation, such as varying time delay, system architectures, and the bilateral control strategies. Thus, we consider the degree of transparency to be achieved when system stability is guaranteed. By combining Eqs. (3.28) and (3.29), we can obtain the impedance transfer function as

$$T(s) = \frac{Z_t}{Z_e} \quad (3.31)$$

We can then analyze the degree of transparency by finding the magnitude and phase response of Eq.(3.31) in frequency domain.

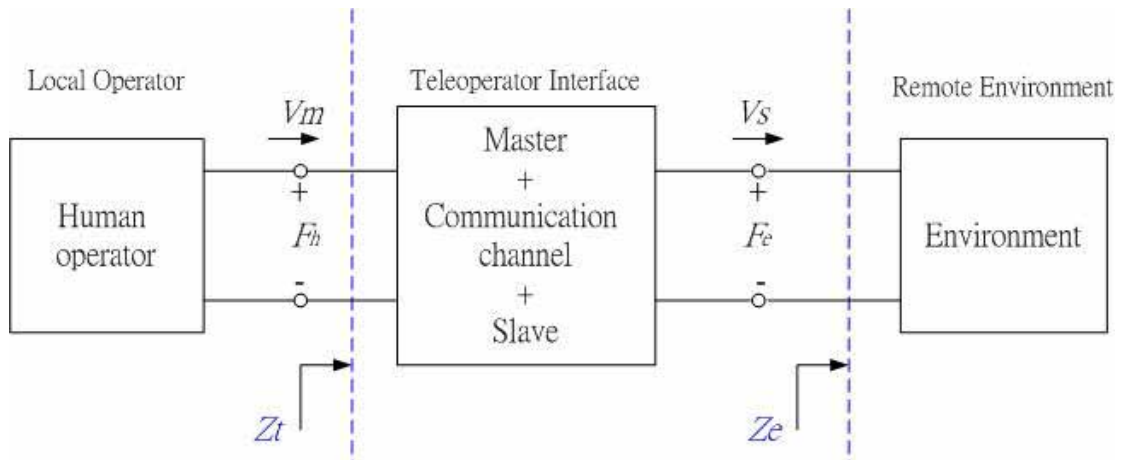
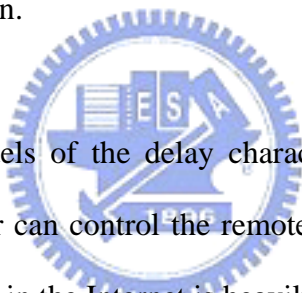


Fig. 3.2 A two-port representation of a telerobotic system.

### 3.5 Synchronicity

The use of Internet to support the communication between the master and the slave is quite attractive due to its worldwide availability. However, the bandwidth limitation and the varying time delay inherent to communication networks can obstruct a system to meet the real-time requirement. Although Transmission Communication Protocol (TCP) can handle the loss of packets, it is still unsuitable for real-time application because of the inherent varying time delay in its transmission mechanism. For instance, if the messages are lost, TCP attempts to recover it by retransmission until it is correctly received and delays any received messages until they can be delivered by the same order they were sent. This kind of mechanism is not desired for real time application.



Some mathematical models of the delay characteristics in Internet have been developed so that the operator can control the remote robot system more accurately. However, the packet exchange in the Internet is heavily affected by the packets' routes and routing algorithms at each node they traverse. Therefore, it is extremely difficult to directly compensate for the randomness of time delay to achieve real-time teleoperation. Besides, some other communication protocols, like Real-time Transport Protocol (RTP), have been applied for real-time applications. However, these protocols still do not meet the true real-time requirements because they only support a best-effort service on a first-come, first-served basis. There is still a long way to go to develop a real-time interactive teleoperation system.

### 3.6 Event-based teleoperation system

Because the asynchronous between the master and slave is mainly due to the varying time delay in the communication links, some researchers suggest that if a non-time based action reference variable instead of time is used to drive the system, it would become immune to time delay. Generally, this action non-time reference is called event. The event-based controller design is first introduced in [29]. Several studies and applications followed [28,6-9]. In this section, we utilize the concept of the event-based control to develop an event-based teleoperation system for system performance comparison with the proposed scheme. In event-based control, time is no longer a synchronized reference. A non-time-based action reference, usually denoted by  $s$ , is used to replace time as the action reference in the system. For a path-based approach described in [28], with a predefined given path  $S$ , shown in Fig. 3.3, we can obtain the current value of action reference value  $s$  by measuring the current output of the robot system. Let  $y_1$  be a measurement of the robot position, and the point  $s_1$  correspond to a point in the given path that has the minimum distance from  $y_1$  to the given path, that is, the orthogonal projection of  $y_1$  to the given path. The path-based action reference  $s$  is then defined as the distance traveled from  $s_0$  to  $s_1$  along the given path  $S$ . Based on  $s$ , a desired input  $y^d(s)$  can be obtained from path-based motion plans [28]. However, when the event-based control is used for bilateral teleoperation system, there is no predefined path, since the path is generated in real-time by the operator based on the feedback received. Thus, some modification has to be made, as described below.

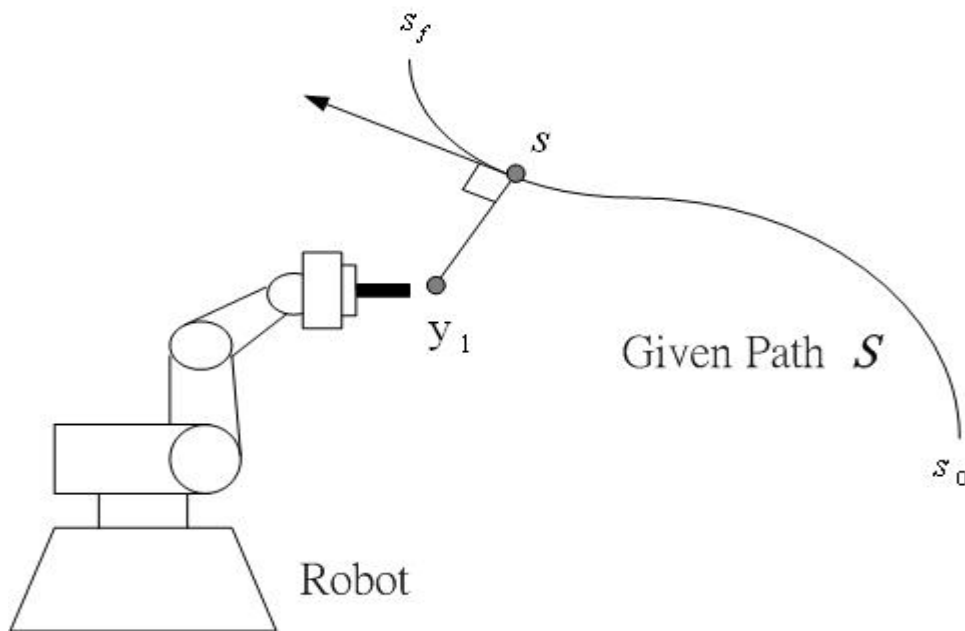


Fig. 3.3 A diagram of action reference for path-based control.



### 3.6.1 Event-based control for teleoperation system

We have developed an event-based teleoperation system, with its system architecture shown in Fig. 3.4, where  $F_h(s)$ ,  $X_m(s)$  and  $V_m(s)$  denote operating force, position and velocity commands, respectively,  $F_e(s)$  denotes the measurement of contact force between the slave and environment at current event,  $s$  denotes the event in an event-based teleoperation system, which is chosen as the command number. Based on the desired position and velocity commands, the developed discrete sliding-mode controller is used to generate proper control input to move the slave of the event-based teleoperation system.

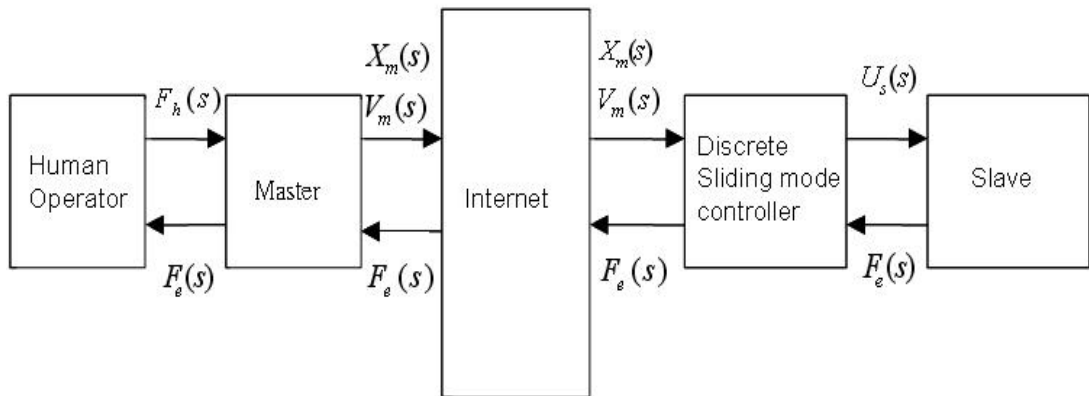


Fig. 3.4 System architecture of the event-based teleoperation system

For illustration, Fig. 3.5 shows the flowchart of the algorithm for this event-based teleoperation system. The position and velocity commands generated by the master are sent to the remote site via the internet, the next event's commands will not be generated until the most up-to-date force is received at the local site. Thus, the system is always synchronized in event, but not synchronized in time, because the slave manipulator needs to wait for each event's command arrive from the master to execute the task. It thus only eliminates the buffering effect that makes the signal flowing in the network invoked by time delay to achieve system synchronicity in event aspect. When the communication delay becomes lager, the slave may exhibit much unsmooth behavior and the measured contact force for the human operator be distorted severely.

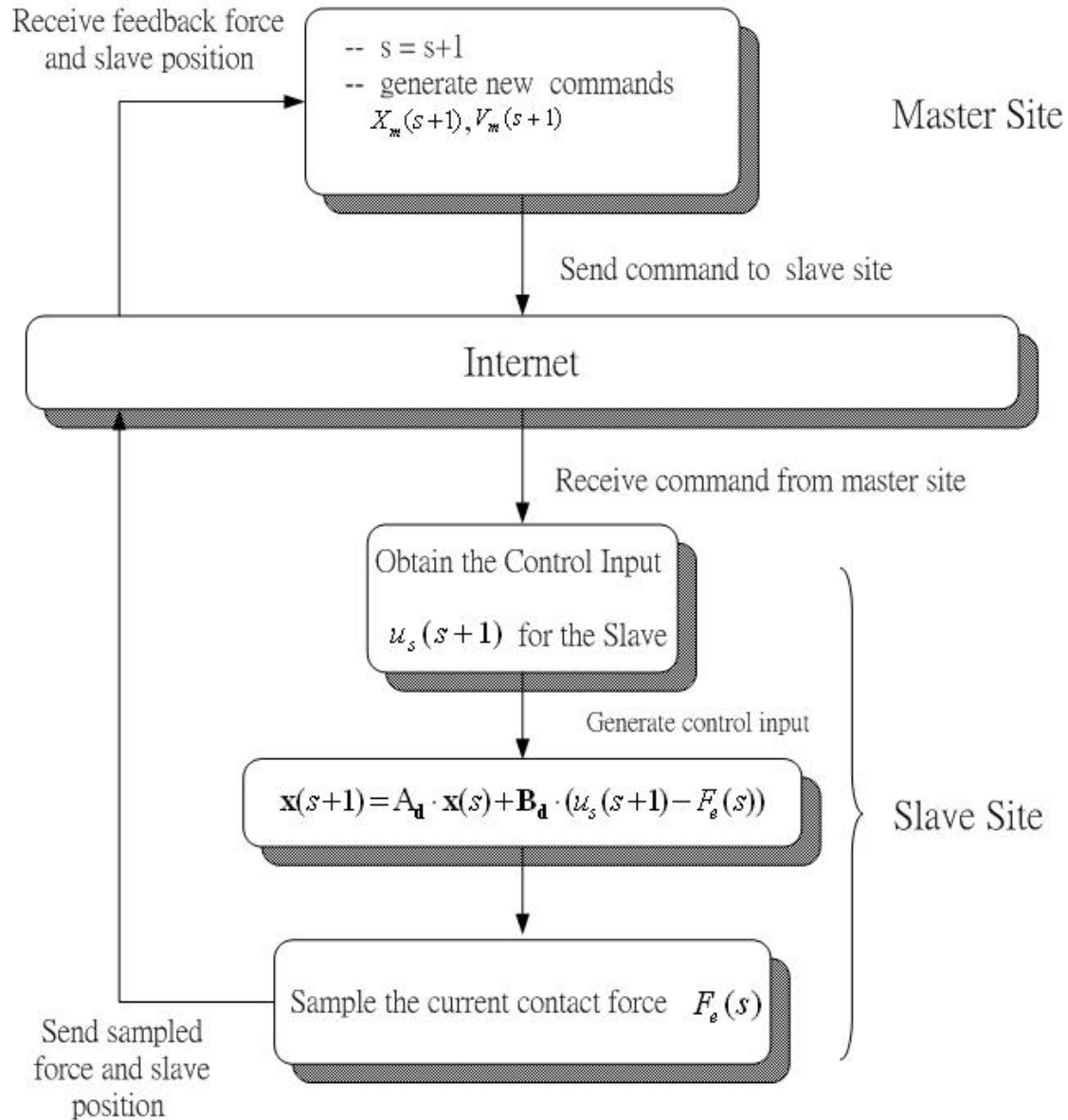


Fig. 3.5 Flowchart of the algorithm for the event-based teleoperation system.

For this event-based system, we use the same single DOF master/slave dynamic model described in Eqs. (2.2) and (2.3). The dynamics of the master in event-domain is then described as

$$\mathbf{M}_m \dot{V}_m(s) + \mathbf{B}_m V_m(s) = F_h(s) - F_e(s-1), \quad s = 0, 1, 2, \dots \quad (3.32)$$

The position and velocity command can be obtained by sampling the value of the master position and velocity at the time a new event happens. Because the event-based teleoperation system is triggered by event instead of time, it acts like a

discrete time system, such that the continuous type of slave controller is not adequate to be used in the event-based teleoperation system. The design for control input is described as follows.

By letting state variables be  $x_1 = x_s(t)$ ,  $x_2 = \dot{x}_s(t)$ , we can obtain the state equation of the slave as

$$\begin{aligned} \dot{\mathbf{x}} = \begin{bmatrix} \dot{x}_1 \\ \dot{x}_2 \end{bmatrix} &= \begin{bmatrix} 0 & 1 \\ 0 & -\frac{\mathbf{B}_s}{\mathbf{M}_s} \end{bmatrix} \begin{bmatrix} x_1 \\ x_2 \end{bmatrix} + \begin{bmatrix} 0 \\ \frac{1}{\mathbf{M}_s} \end{bmatrix} (u_s(t) - f_e(t)) \\ &= \mathbf{A} \cdot \mathbf{x}(t) + \mathbf{B} \cdot (u_s(t) - f_e(t)) \end{aligned} \quad (3.33)$$

Then, by digitalizing the continuous form of the state equation in Eq.(3.33), we can obtain its discrete form as

$$\mathbf{x}(s+1) = \mathbf{A}_d \cdot \mathbf{x}(s) + \mathbf{B}_d \cdot (u_s(s) - F_e(s)) \quad (3.34)$$

where  $\mathbf{A}_d = e^{\mathbf{A}T}$ ,  $\mathbf{B}_d = \int_0^T e^{\mathbf{A}t} \cdot \mathbf{B} dt$ ,  $s$  denotes the event, and  $T$  sampling period (the round-trip delay in this system). Based on the tasks requirements that the slave should perform both path tracking and impact force reduction, a linear switching function is given as

$$\begin{aligned} s_d(\mathbf{x}) &= k_x [X_s(s) - k_p X_m(s)] + k_v [V_s(s) - k_p V_m(s)] + F_e(s) \\ &= [k_x \quad k_v] \left( \begin{bmatrix} X_s(s) \\ V_s(s) \end{bmatrix} - k_p \begin{bmatrix} X_m(s) \\ V_m(s) \end{bmatrix} \right) + F_e(s) \\ &= \mathbf{C}^T \cdot [\mathbf{x}(s) - k_p \mathbf{x}_d(s)] + F_e(s) \end{aligned} \quad (3.35)$$

where  $k_p$  is a scaling factor for position and velocity commands. Refer to [11], if the reaching law is satisfied as

$$\begin{aligned} s_d(s+1) - s_d(s) &= -qTs_d(s) - \varepsilon T \operatorname{sgn}(s_d(s)), \quad \varepsilon > 0, q > 0 \\ 1 - qT &> 0 \end{aligned} \quad (3.36)$$

the trajectory of the system states will move monotonically toward the switching



plane ( $s_d = 0$ ) and zigzag around it in a finite time. Thus, by substituting Eq.(3.35) into Eq.(3.36), we can obtain Eq.(3.37):

$$\begin{aligned}
s_d(s+1) - s_d(s) &= \mathbf{C}^T [\mathbf{x}(s+1) - k_p \mathbf{x}_d(s+1)] + F_e(s+1) \\
&\quad - \mathbf{C}^T [\mathbf{x}(s) - k_p \mathbf{x}_d(s)] - F_e(s) \\
&= \mathbf{C}^T [\mathbf{A}_d \cdot \mathbf{x}(s) + \mathbf{B}_d \cdot (u_s(s) - F_e(s)) - k_p \mathbf{x}_d(s+1)] \\
&\quad + F_e(s+1) - \mathbf{C}^T \mathbf{x}(s) + k_p \mathbf{C}^T \mathbf{x}_d(s) - F_e(s) \\
&= -qTs_d(s) - \varepsilon T \operatorname{sgn}(s_d(s))
\end{aligned} \tag{3.37}$$

By further substituting Eq.(3.34) into Eq.(3.37) for solving  $u_s(s)$ , we can obtain the control law of the event-based teleoperation system as

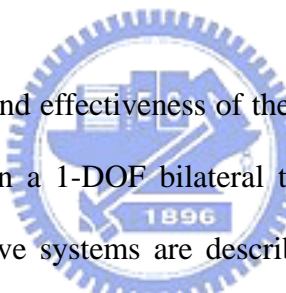
$$\begin{aligned}
u_s(s) &= -(\mathbf{C}^T \mathbf{B}_d)^{-1} [\mathbf{C}^T \mathbf{A}_d \mathbf{x}(s) - \mathbf{C}^T \mathbf{x}(s) \\
&\quad + qTs_d(s) + \varepsilon T \operatorname{sgn}(s_d(s))] + F_e(s)
\end{aligned} \tag{3.38}$$

Here, we neglect  $k_p \mathbf{C}^T (x_d(s) - x_d(s+1))$  and  $(F_e(s+1) - F_e(s))$  terms to simplify the derivation, because they can be compensated for by selecting  $\varepsilon$  and  $q$  properly.



## Chapter 4

### Simulations



To verify the feasibility and effectiveness of the proposed scheme, we perform a series of simulations based on a 1-DOF bilateral telerobotic system. The dynamic models of the master and slave systems are described in Eqs. (2.2) and (2.3). The plant model uncertainty is neglected and assumed to be zero for concerning only the time delay effect on the bilateral telerobotic system. In the following simulations, the plant parameters are set to be  $M_m = 0.5Kg$  and  $B_m = 1.5Ns/m$  for the master, and  $M_s = 5Kg$  and  $B_s = 1.5Ns/m$  for the slave. For the impedance controller on the master, the desired impedance parameters described in Eq.(3.1) are set to be  $M = 0.02Kg$ ,  $B = 0.5Ns/m$ , and  $K = 0.04N/m$ . For the sliding-mode-impedance controller on the slave, the desired impedance parameters described in Eq.(3.3) are set to be  $\bar{m}_s = 0.05Kg$ ,  $\bar{b}_s = 2.1Ns/m$ , and  $\bar{k}_s = 80N/m$ . The constant position and force scaling factors are set to be  $K_p = 1$  and  $K_f = 1$ , respectively. The boundary layer thickness and nonlinear gain of the sliding-mode-impedance controller are set to

be  $\varepsilon = 0.1$  and  $K_g = 20$ , respectively. In the simulations, the compliance task to execute is to manipulate the slave to contact with a wall. The impedance controller is installed on the master to reduce the force imposed on the master, and the sliding-mode-impedance controller is installed on the slave to track the movement of the master and maintain a stable contact force. We input into the master commands in the form of a sinusoidal function. The output responses are the positions and contact forces of the slave.

#### 4.1 Matlab simulation

The PC used for Matlab simulations is P4—2GHz and 256 DDRAM. The operating system and the version of Matlab simulator are Microsoft Windows XP and Matlab ver.6.5, respectively. As the first set of simulations, Fig. 4.1 shows the simulation results in performing the task of interacting with a wall under no time delay condition. Fig. 4.1(a) shows the positions of the master and slave, Fig. 4.1(b) the feedback force for the master and contact force for the slave, and Figs. 4.1(c)-(d) the magnitude of slave and master control inputs, respectively. Because the time delay was not included in the simulation, the positions of the slave followed that of the master closely, contact and reflection forces were very close, and the control inputs for the slave did not invoke chattering, as expected.

In the second set of simulations, we added into the system a constant time delay. The same compliance task described above was executed. Fig. 4.2 shows the result under constant time delay. We set the forward and backward delay to a constant value of 300 msec and 250 msec, respectively. Fig. 4.2(a) shows that the positions of the slave did follow that of the master after a period of time. Fig. 4.2(b) shows the

waveform of contact forces and feedback forces were the same under constant time delay. The contact force was stable during the compliance task. Figs. 4.2(c)-(d) show the magnitudes of control inputs for the slave and master, respectively.

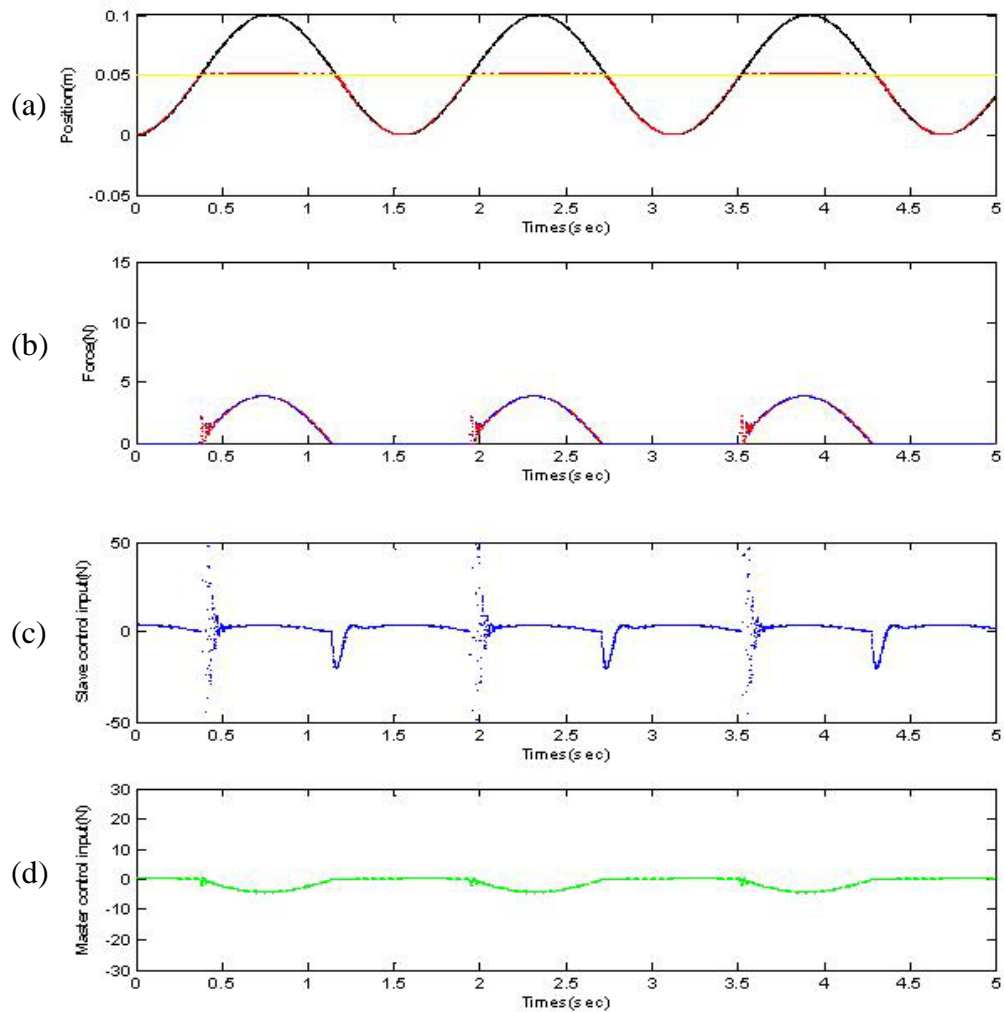


Fig. 4.1 Position and force responses of the proposed scheme without time delay: (a) position response (black: master, yellow: wall, red: slave), (b) force response (blue: contact force, red: reflection force), (c) control input for the slave, and (d) control input for the master.

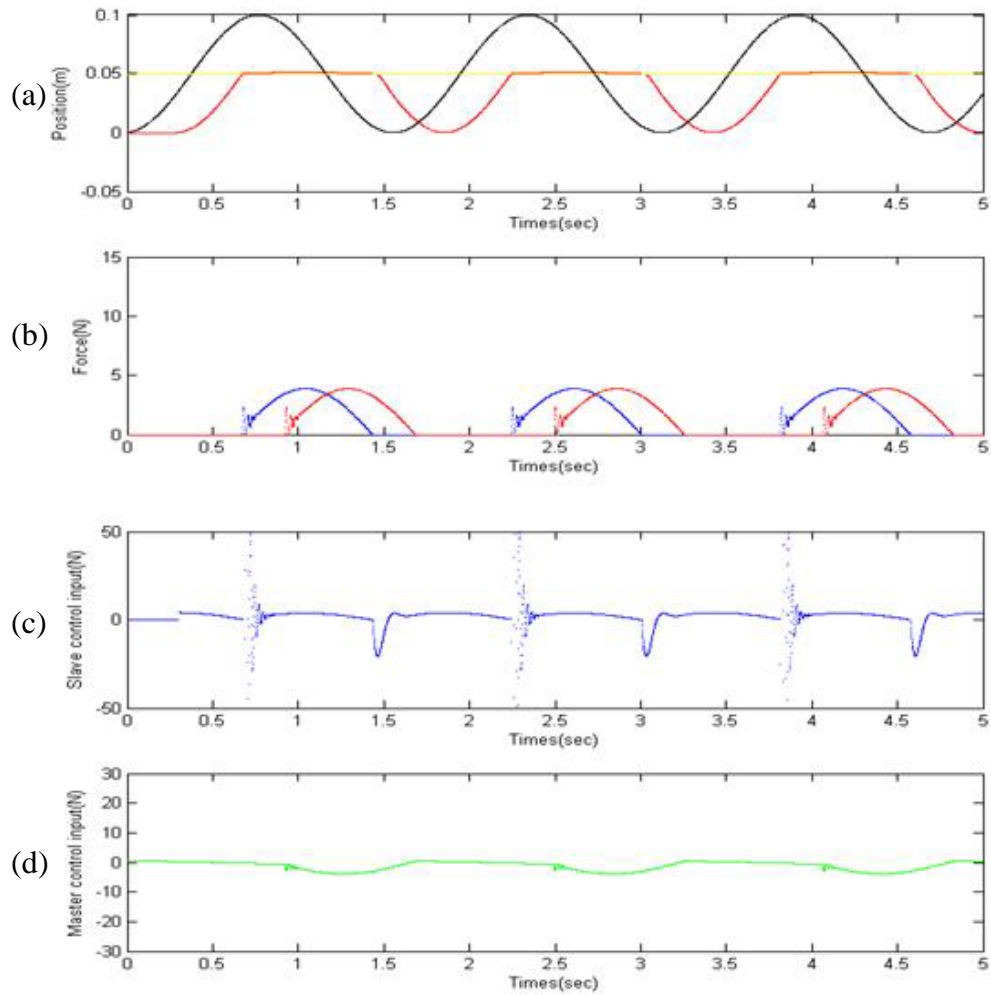


Fig. 4.2 Position and force responses of the proposed scheme under constant time delay: (a) position response (black: master, yellow: wall, red: slave), (b) force response (blue: contact force, red: feedback force), (c) slave control input, and (d) master control input.

In the third set of simulations, we let the bilateral time delay vary with time. We assumed that the forward delay varied from 30 to 50 msec and backward delay from 40 to 60 msec. Fig. 4.3 shows the simulation results under this delay condition. Fig. 4.3 (a)-(b) shows the forward and backward delay profiles generated by the Matlab simulator, respectively. Fig. 4.3(c) shows the master and slave position responses. The contact and feedback forces were shown in Fig. 4.3(d). We found that the slave followed the master closely in unconstrained motion after a period of time and maintained stable contact force in constrained motion under this delay condition.

Fig. 4.4 shows the simulation results under a larger varying bilateral delay. We assumed that the forward delay varied from 150 to 250 msec and backward delay from 200 to 300 msec; Figs. 4.4(a)-(b) show the forward and backward delay profiles generated by Matlab simulator, respectively. Figs. 4.4(c)-(d) show the positions response and the force responses, respectively. By comparing Fig. 4.3 with Fig. 4.4, we found that even under much large varying time delay, the performance of the proposed scheme did not degrade much. The simulation results in Fig. 4.4 show that the proposed scheme was robust under large varying time delay.

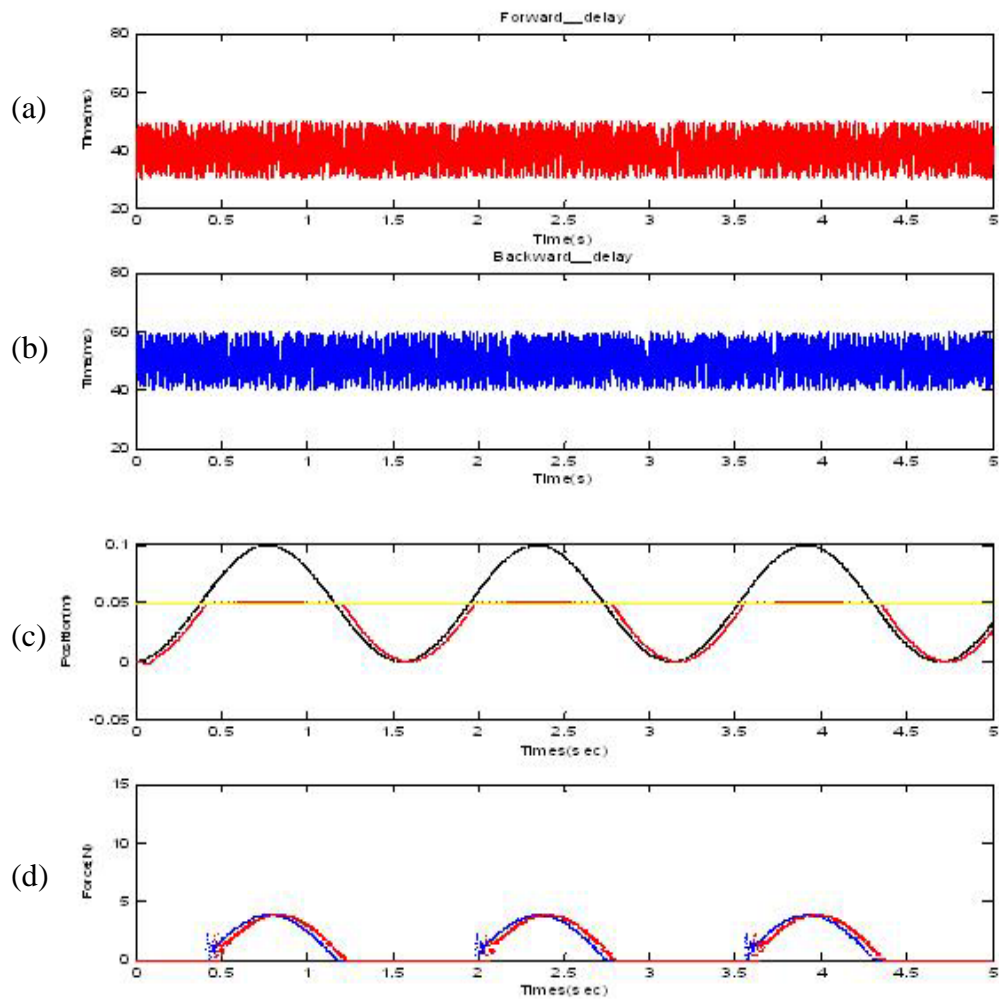


Fig 4.3 Position and force responses of the proposed scheme under varying time delay: (a) the profile of forward delay, (b) the profile of backward delay, (c) position response (black: master, yellow: wall, red: slave), and (d) force response ( blue: contact force, red: feedback force).

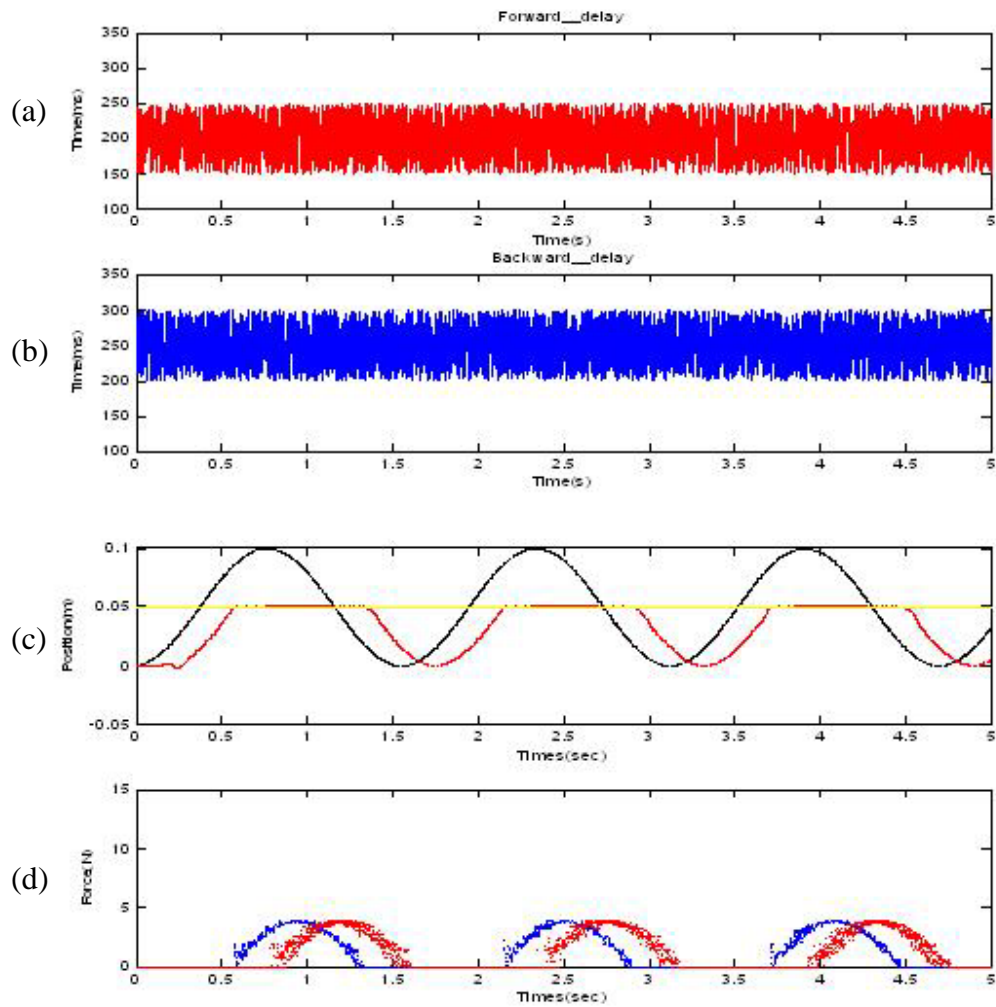


Fig 4.4 Position and force responses of the proposed scheme under larger varying time delay: (a) the profile of forward delay, (b) the profile of backward delay (c) position response (black: master, yellow: wall, red: slave), and (d) force response (blue: contact force, red: feedback force).



## 4.2 VR-based predictive display

In this section, the VR-based predictive display together with virtual force reflection is used to provide real-time prediction of slave position and virtual force reflection at the master site. With the assumptions that the models of the slave manipulator and remote environment in the VR simulator well approximated the actual ones, we intend to show that realistic feel of the remote environment can be achieved. Fig. 4.5 shows the simulation results of including VR-based predictive display in the proposed scheme when the same compliance task that moved the slave to contact with a wall was executed. Figs. 4.5(a)-(c) show the master position, predicted position, and predicted force, respectively, and Figs. 4.5(d)-(f) the slave position, contact force, and feedback force response, respectively. In Figs. 4.5(b)-(c), we found that the predicted position was not with lag and the predicted force reflection provided from the VR simulator did not vibrate. Figs. 4.5(d)-(f) show the position of the slave with small lag and the feedback force vibrated a little bit due to varying time delay. By comparing Fig. 4.5(c) with Fig. 4.5(f), we found that the shape of force responses were almost the same under varying time delay, implying that we successfully incorporate the predicted force reflection into the control loop for providing real-time force reflection and did not destabilize the system. Thus, with the VR-based predictive display, the synchronicity in position and force were achieved between the master and virtual environment. In addition, the human operator could observe the movement of the virtual robot and feel the virtual contact force in real-time with no influence from varying time delay. However, we also considered that this method did not really achieve system synchronicity since the slave position and feedback force were still with lag phenomena. The human operator generated the commands depending on the feedback information from the VR simulator. Thus, if

the predicted position and force were not correctly provided by the VR simulator, improper commands would be generated by the human operator to move the remote slave manipulator. Thus, in this system architecture, we must make sure that the models of the slave and environment constructed in the VR simulator approximates the real ones as close as possible, which is certainly a challenge to overcome.

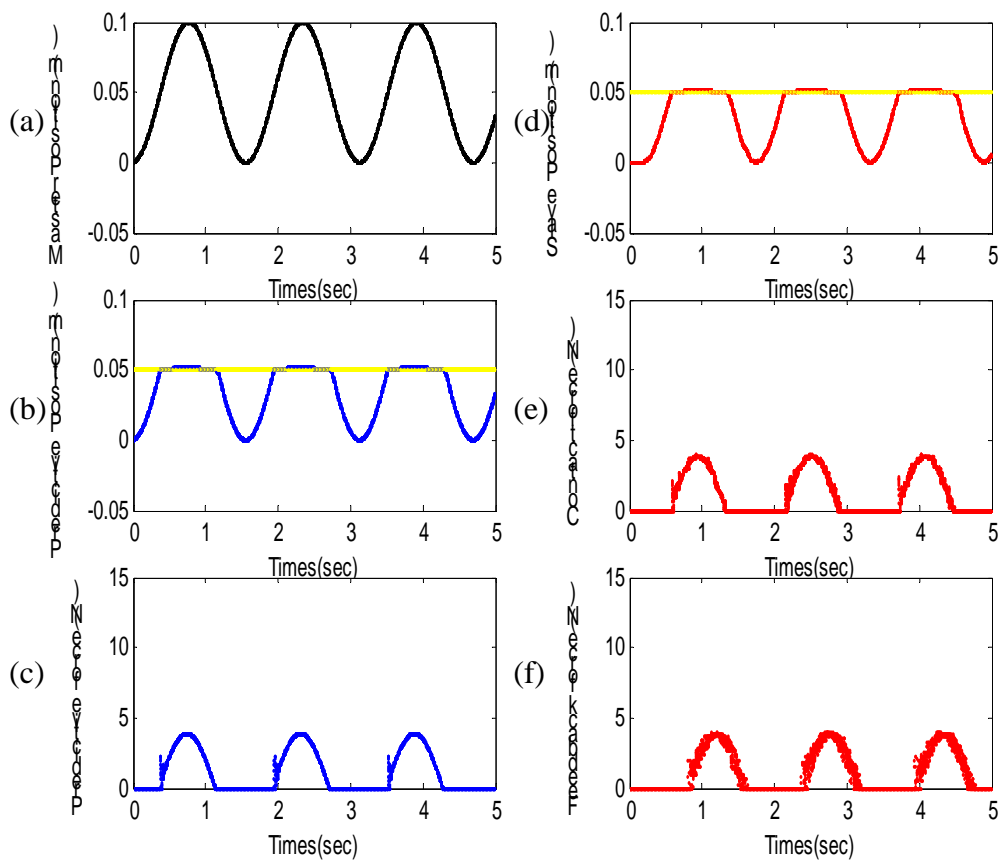


Fig. 4.5 Position and force responses of the master and slave using the VR-based predictive display: (a) position response for the master, (b) position response for the predictive display, (c) force response for the predictive display, (d) position response for the slave, (e) force response for the slave, and (f) feedback force response.

### 4.3 Transparency

In this section, we analyze system transparency from frequency aspect. We utilize the impedance transfer function described in Eq.(3.31) to analyze transparency. We consider only the stiffness of the remote environment. The same compliance task described Sec. 4.1-4.2 was performed. The environmental impedance encountered by the slave is formulated as

$$Z_e = \frac{F_e(s)}{V_s(s)} = \frac{K_e}{s} \quad (4.1)$$

where  $K_e$  denotes the stiffness of the remote environment (a wall).

Fig. 4.6 shows the simulation results of letting the slave manipulator contact with a hard wall with the stiffness set to be  $k_e = 1000N/m$ . Figs. 4.6(a)-(b) show the magnitude and phase responses of the impedance transfer function, respectively. Fig. 4.7 shows the simulation results of letting the slave manipulator contact with a soft wall with the stiffness set to be  $k_e = 100N/m$ . Figs. 4.7(a)-(b) show the magnitude and phase responses of the impedance transfer function, respectively. The forward and backward delays for the simulations in Figs. 4.6 and 4.7 were both set to be 25 msec.

By examining the magnitude and phase responses shown in Figs. 4.6 and 4.7, we found that complete transparency was not achieved. Nevertheless, the proposed scheme preserved a scaled environmental impedance to the operator during compliance tasks in the presence of time delay. Figs. 4.6 and 4.7 show that the transmitted impedance,  $Z_t$ , and the environment impedance,  $Z_e$ , have almost linear and scaled relationship between each other over the bandwidth of human capability. The abrupt variation of magnitude and phase response of the impedance transfer

function in high frequency was mainly due to the delay effect. In Figs. 4.6 and 4.7, we found that the delay effect did not degrade the system transparency obviously in the bandwidth of human capability. We concluded that the scaled “feel” of the remote environment was preserved.

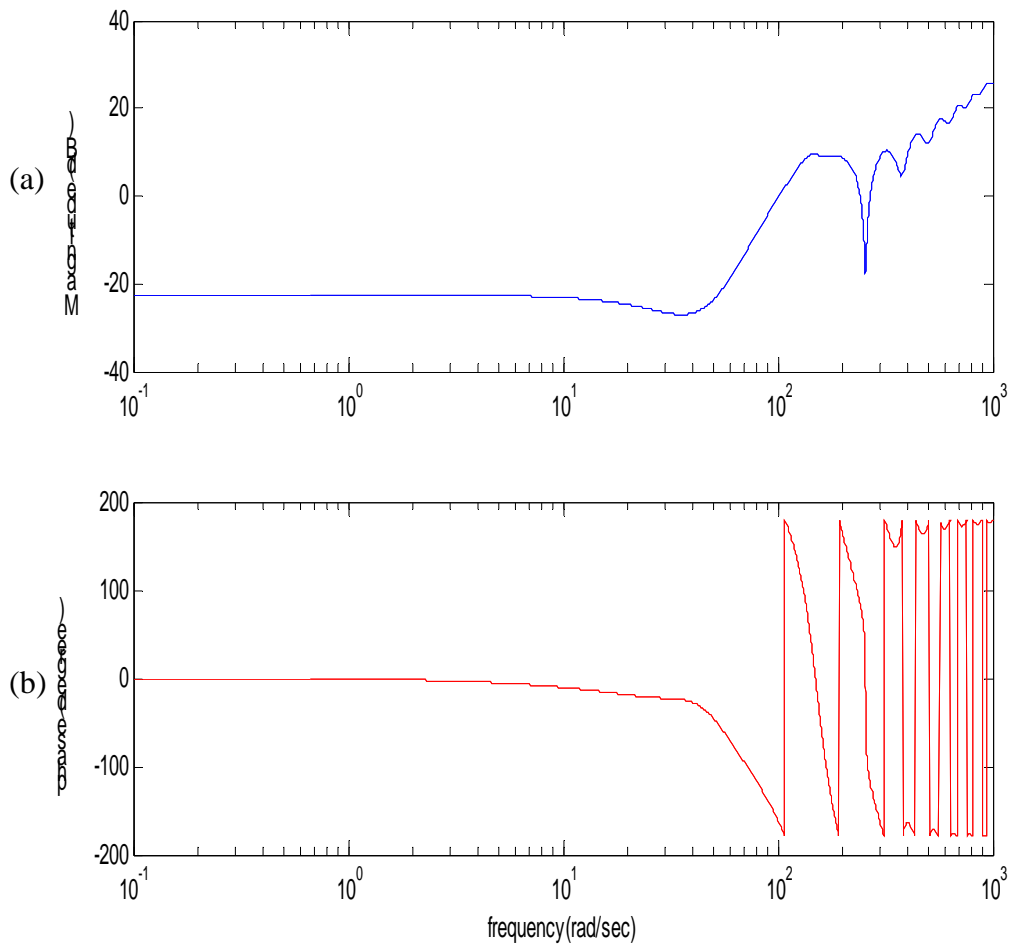


Fig. 4.6 Magnitude and phase responses of the impedance transfer function when contact with hard wall: (a) magnitude response and (b) phase response.

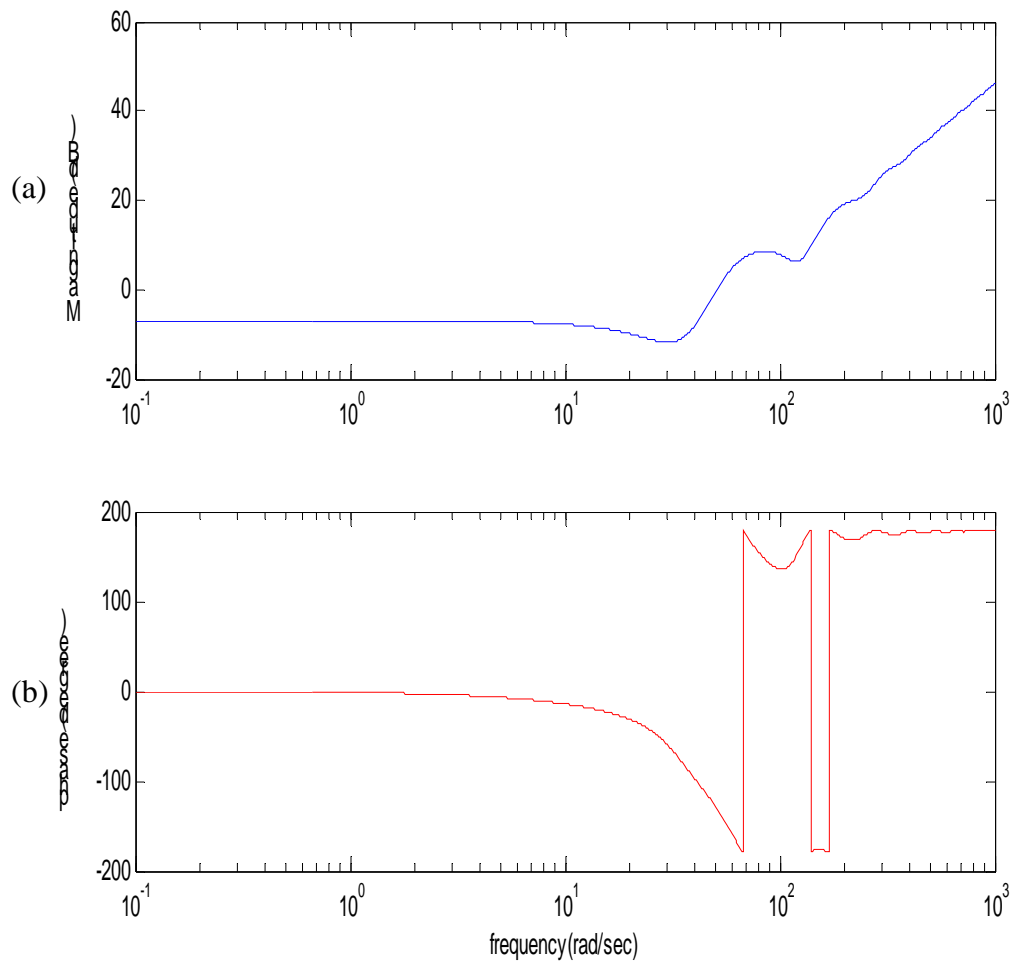
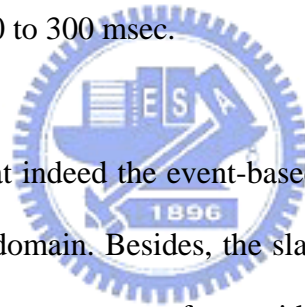


Fig. 4.7 Magnitude and phase responses of the impedance transfer function when contact with soft wall: (a) magnitude response and (b) phase response.

## 4.4 Event-based teleoperation system

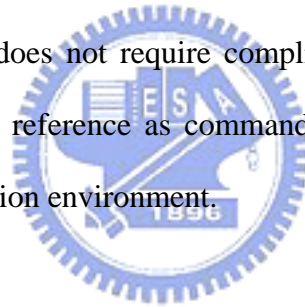
In this section, simulations were performed to evaluate the performance of the event-based system we have developed in Sec. 3.6. Fig. 4.8 shows the simulation results of the of the event-based teleoperation system in the presence of varying time delay in event domain. Figs. 4.8(a)-(c) show the position and force response and Fig. 4.8(d) the plot of time versus  $s$ , the event. In this set of simulations, the system position scaling factor was set to be  $k_p = 1$ . The control parameters described in Eq.(3.35) were set to be  $k_x = 200N/m$  and  $k_v = 2Ns/m$ , respectively. The parameters  $\varepsilon$  and  $q$  described in Eq.(3.36) were set to be  $\varepsilon = 0.01$  and  $q = 0.25$ , respectively. The forward delay was set to vary from 150 to 250 msec and the backward delay vary from 200 to 300 msec.



In Fig. 4.8, we found that indeed the event-based teleoperation system achieved event-synchronicity in event domain. Besides, the slave followed the master position commands and maintained a proper contact force with the event-based controller. Fig. 4.9 shows the simulation results in time domain (from 20 to 45 secs), which is a zoom-in version of Fig. 4.8. Fig. 4.9(a) shows the master position commands of each event generated from the human operator, and the slave position response in each event in time domain. Fig. 4.9(b) shows the measured contact force. Fig. 4.9(c) shows the feedback force from the slave. In Fig. 4.9, we found that in the event-based system the time-synchronicity was not achieved. The slave position response and the feedback force were still with lag under network transmission. It only achieved event synchronization.

In the event-based teleoperation system, it only concerns about whether the slave

states followed the master commands at each event. The slave states during the intervals between two events were not the main consideration. From Sec. 3.6, it is clear that the frequency of event is a function of time delay (if the round-trip delay is 0.5sec, the frequency of events is 2 events/sec). Since we have an event per round-trip delay, then the frequency by which the force measured and fed back is a function of time delay. This implies that the force is sampled once for each round-trip delay and since this delay is variable then the sampling rate of force is variable. If the time delay is large, the sampling rate of the actual contact force decreases. Thus, the measured force signal reconstructed at the master as force reflection for the human operator would much differ from the actual contact force, yielding unnatural feeling to the human operator and degrading the realism. The event-based control method is extensively used, though. It does not require complicated mathematical knowledge because the chosen of action reference as command cycle is intuitive, simple, and suitable for network transmission environment.



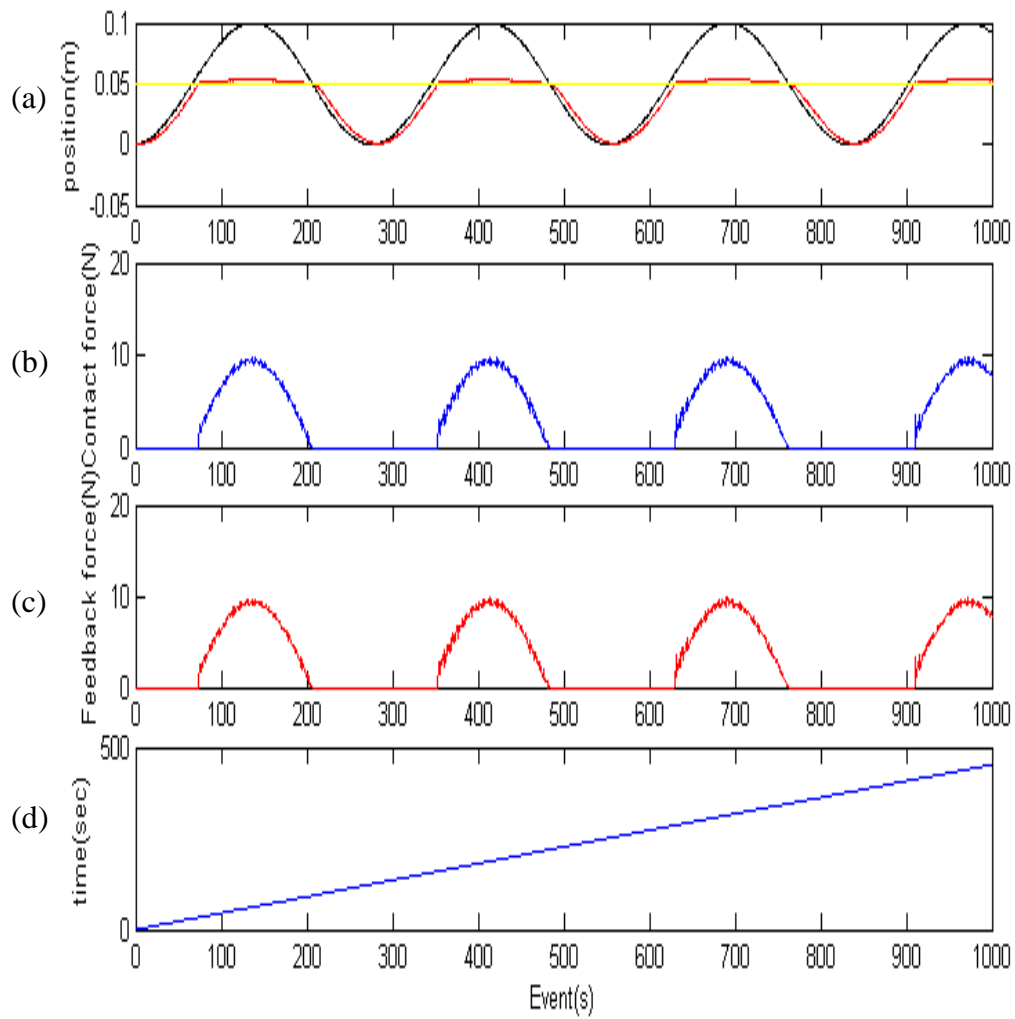


Fig. 4.8 Position and force responses of the event-based teleoperation system in event domain: (a) position response (black: master, red: slave, yellow: wall), (b) contact force, (c) feedback force, and (d) time versus event.



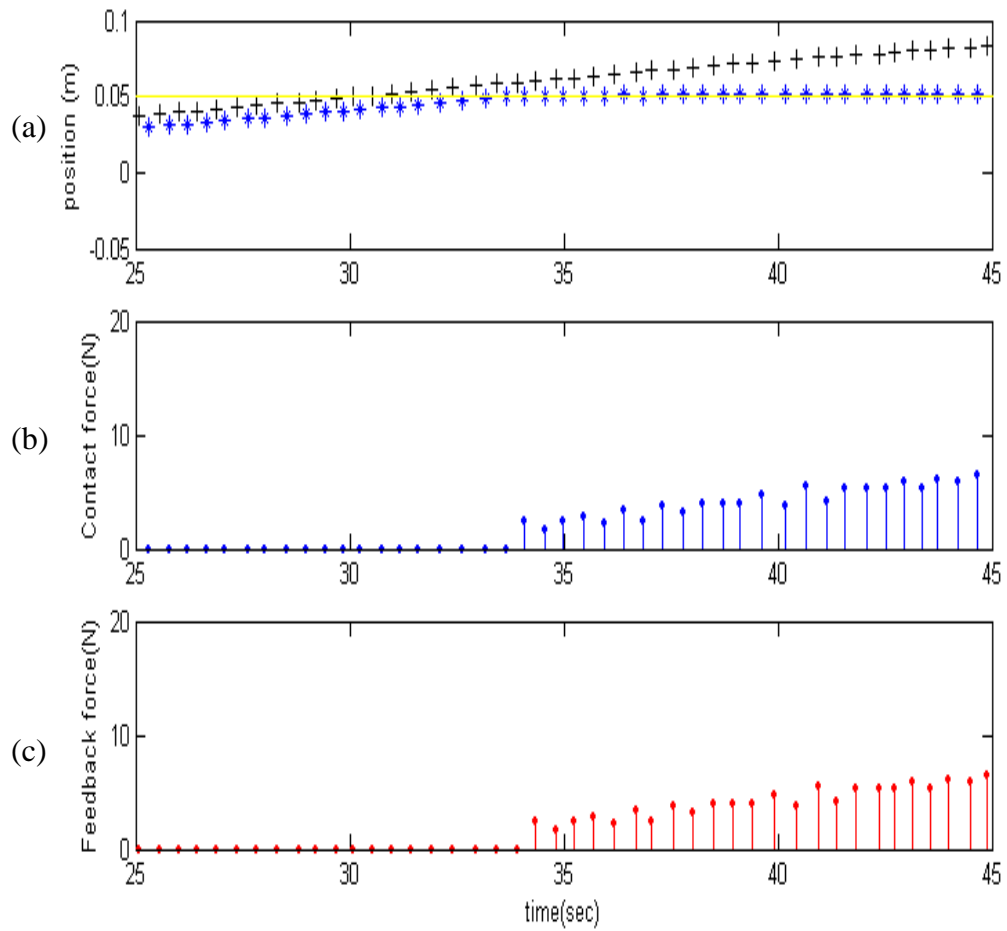
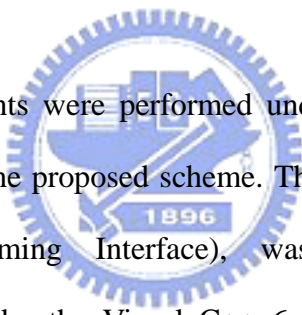


Fig. 4.9 Position and force responses of the event-based teleoperation system in time domain: (a) position response (black +: master, blue \* : slave, yellow: wall), (b) Measured force, and (c) feedback force.

## Chapter 5

### Experiments

The logo of National Chiao Tung University is a circular emblem. It features a gear-like outer border. Inside the circle, there is a stylized building or structure. At the bottom of the emblem, the year '1896' is inscribed.

The following experiments were performed under real network connection to evaluate the performance of the proposed scheme. The Winsock, one of the network API (Application Programming Interface), was used as the networking communication software. Under the Visual C++ 6 programming environment, we initialized Windows sockets and created the connection between the master and slave site's computers with Winsock functions. A socket is a communication endpoint. When both computers start to communicate, each one can use the socket as the interface to connect each other. All of the data flows in the network can be received or sent through these sockets. We first investigated the teleoperation between two computers connected via the Internet in National Chiao Tung University (NCTU). The sampling period of master site PC was 0.001 msec. Thus, there were 5000 position commands generated at the local site and send to remote site for task execution within 5 sec. Fig. 5.1 shows the profile of round-trip delay that each master command encountered during task executed between two computers in NCTU.

Fig. 5.2 shows the Internet experimental results. Figs. 5.2(a)-(c) show the master position, predicted position, and predicted force, respectively, and Figs. 5.2(d)-(f) the slave position, contact force, and feedback force, respectively. In Figs. 5.2(b)-(c), we observed that VR has provided real-time predicted position and force reflection information to the operator, which were almost similar to the actual slave positions and contact forces. Fig. 5.2(d) shows that the slave did follow the master trajectory quite well in free motion. In Fig. 5.2(e), the slave maintained a stable contact force in contact motion. From the results, we concluded that under the small varying time delay between the two computers in NCTU, the system performance was satisfactory.

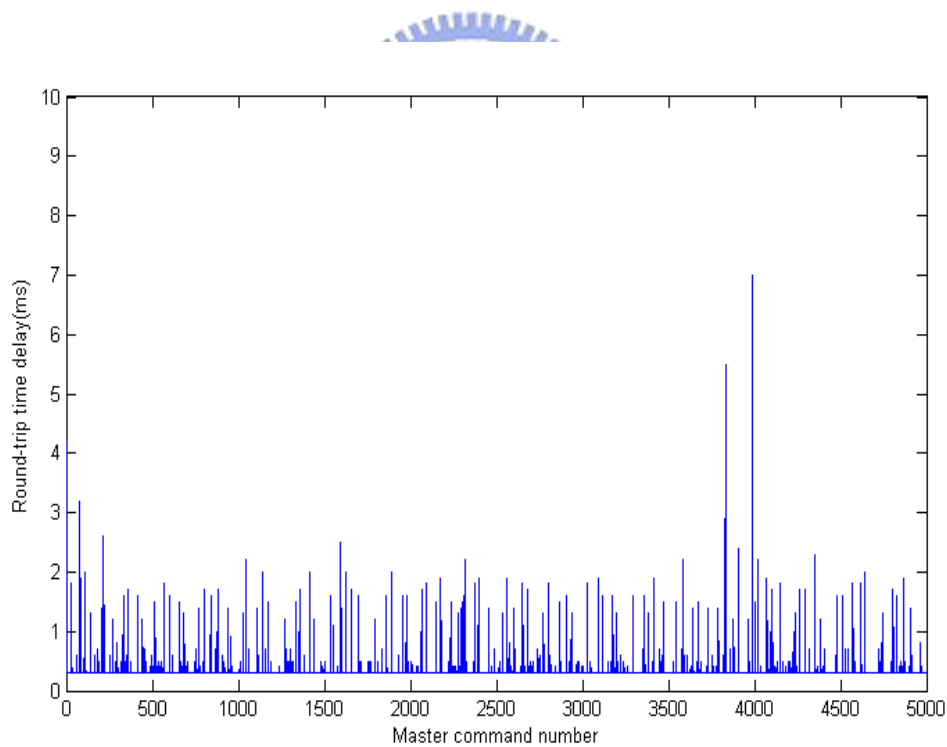


Fig. 5.1 The profile of round-trip delay that each master command encountered between two computers in NCTU.

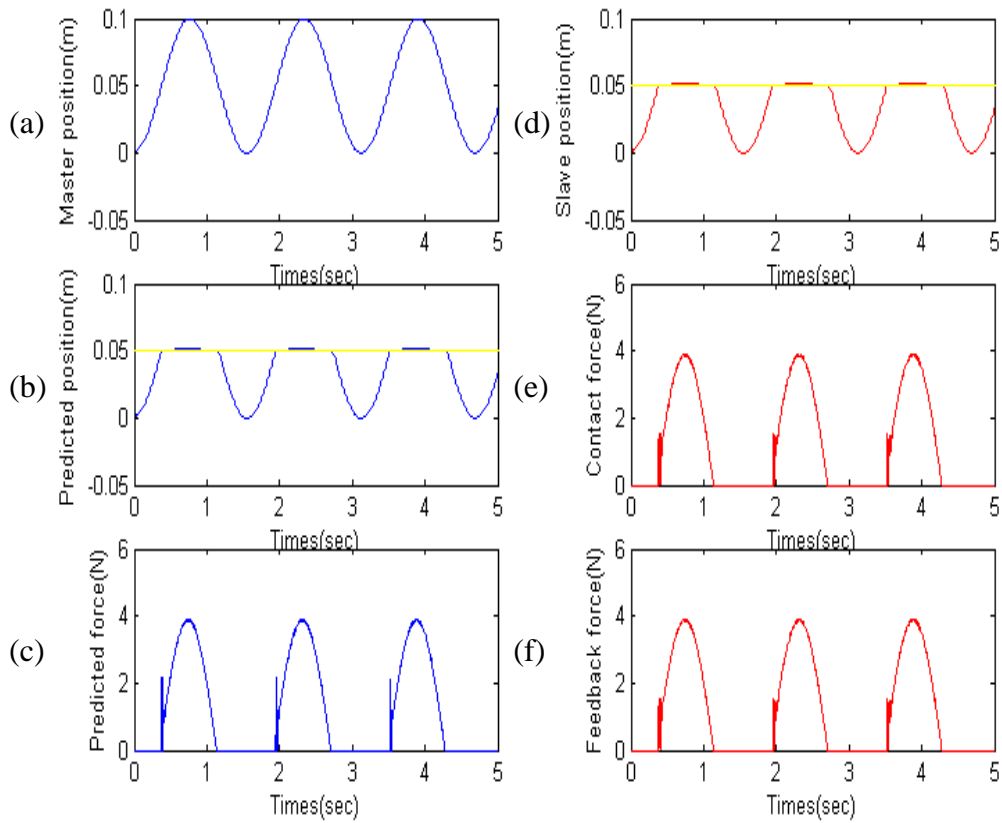


Fig. 5.2 Internet experimental results in performing the compliance task between two computers in NCTU: (a) position of the master, (b) predicted position in the master site, (c) predicted virtual force in the master site, (d) position of the slave, (e) contact force in the slave site, and (f) feedback force from the slave site.

We then executed the task between the computer in our laboratory and that in National Cheng Kung University (NCKU), which is located at southern part of Taiwan. Fig. 5.3 shows the profile of round-trip delay that each master command encountered during task execution between the two computers in NCTU and NCKU. Fig. 5.4 shows the Internet simulation results. We found that the system stability was still maintained and performance was not affected by the larger time delay between NCTU and NCKU.

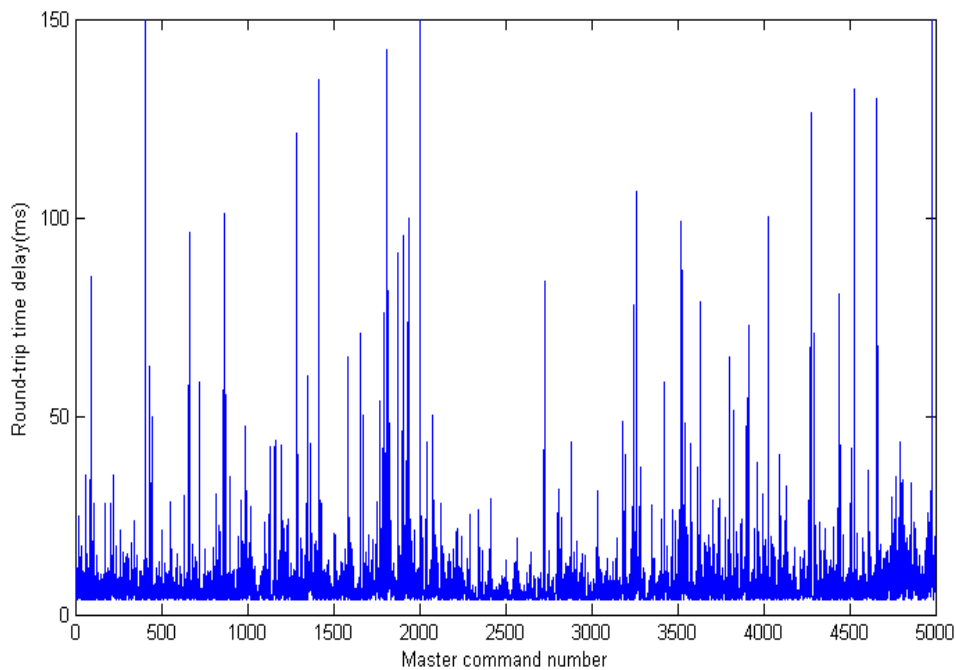


Fig. 5.3 The profile of round-trip delay that each master command encountered between two computers in NCTU and NCKU.

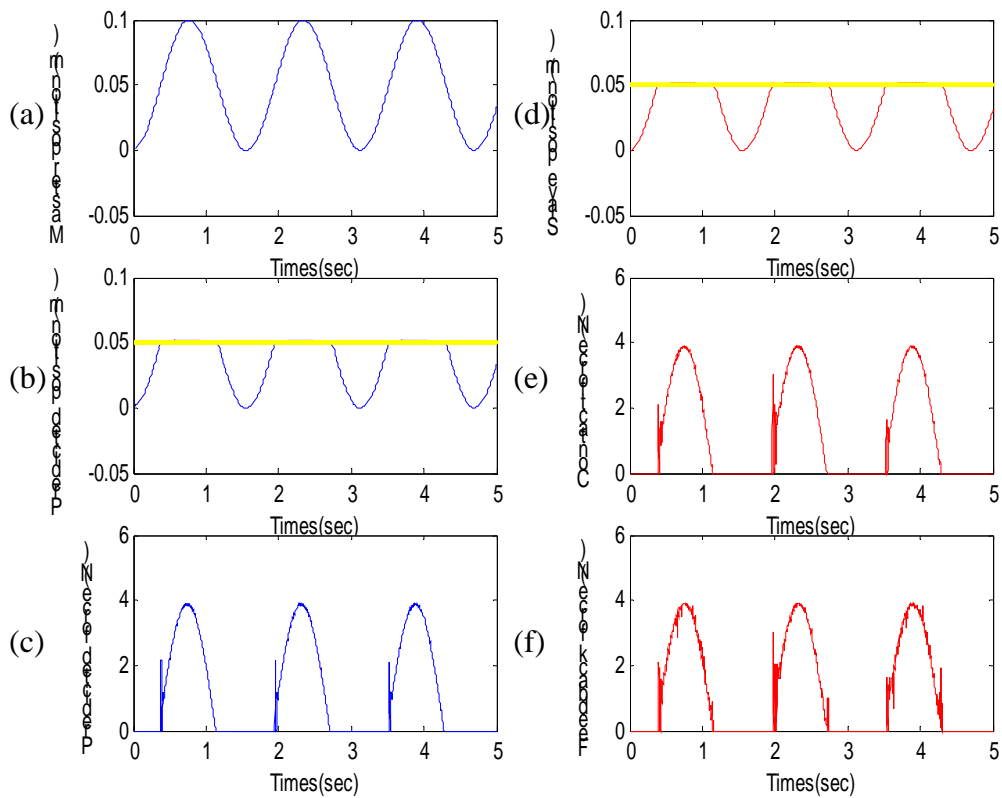


Fig. 5.4 Internet experimental results in performing the compliance task between two computers in NCTU and NCKU: (a) position of the master, (b) predicted position in the master site, (c) predicted virtual force in the master site, (d) position of the slave, (e) contact force in the slave site, and (f) feedback force from the slave site.

In the third set of Internet experiments, we executed the task between the computers in our laboratory and that in Nanotechnology Lab. of UC Irvine, Ca., USA. Fig. 5.5 shows the profile of round-trip delay that each master command encountered during the task executed between the two computers in Taiwan and USA. Fig. 5.6 shows the Internet experimental results. Figs. 5.6(a)-(c) show the master position, predicted position, and predicted force, respectively, and Figs. 5.6(d)-(f) the slave position, contact force, and feedback force, respectively. In Figs. 5.6(b)-(c), we observed that the real-time predicted position and force reflection at the master site still approximated the actual slave position and contact force. Fig. 5.6(d) shows that the slave followed the master trajectory robustly even under much larger varying time delay than previous ones. In Fig. 5.6(e), the stability of contact force in contact motion did not degrade severely. System stability was still maintained and performance almost not affected by the much larger time delay between Taiwan and USA.

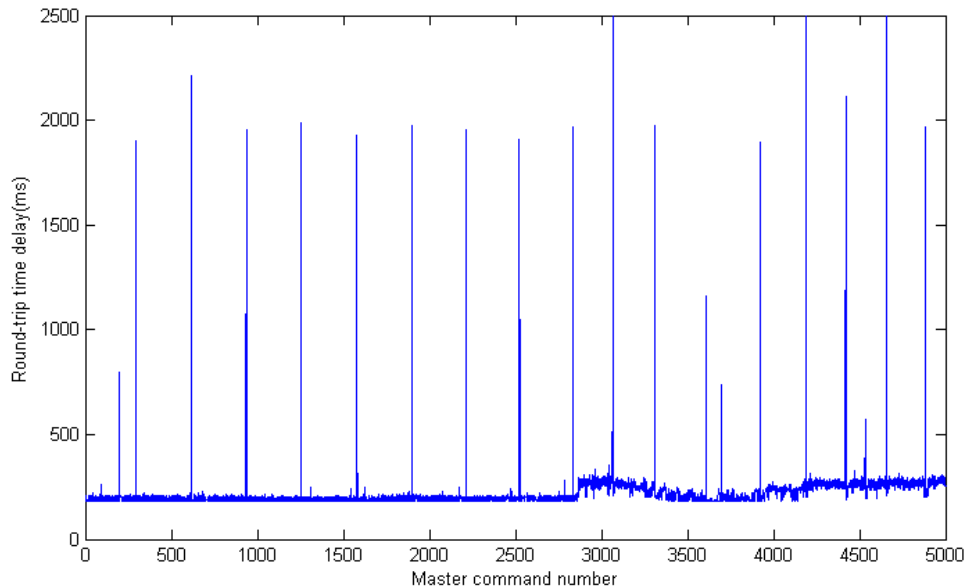
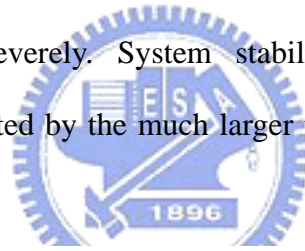


Fig. 5.5 The profile of round-trip delay that each master command encountered between two computers in Taiwan and USA.

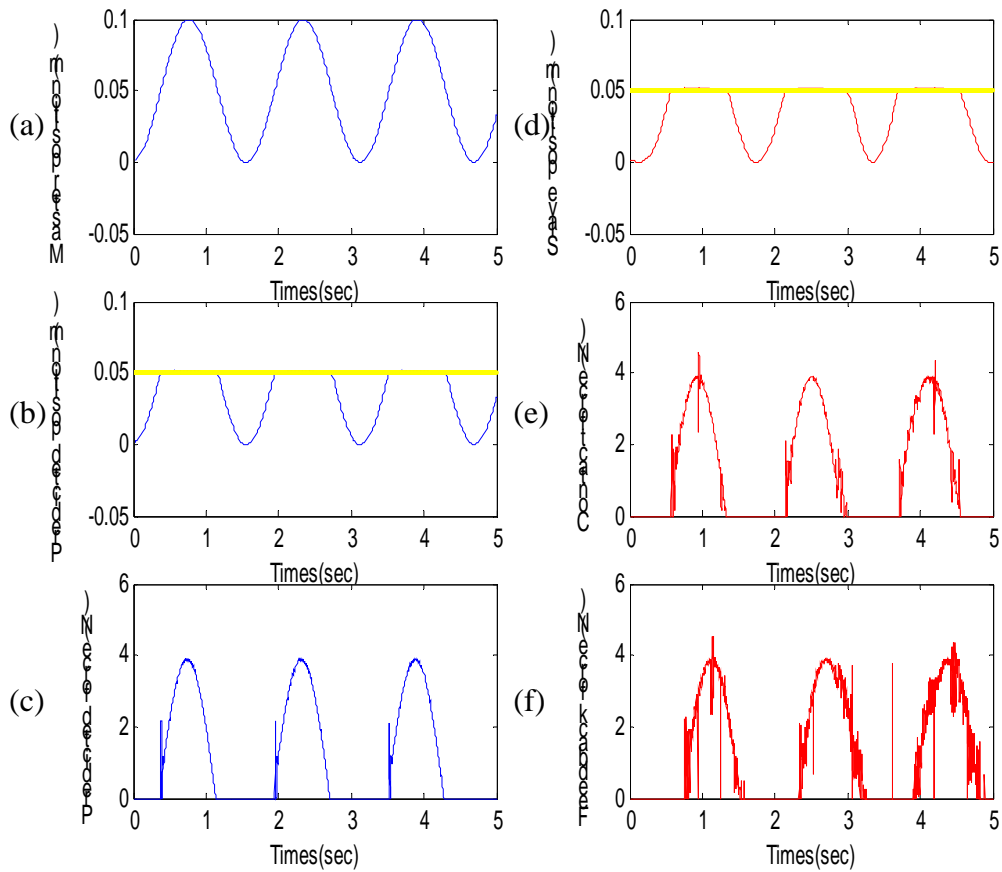


Fig. 5.6 Internet experimental results in performing the compliance task between two computers in Taiwan and USA:(a) position of the master, (b) predicted position in the master site, (c) predicted virtual force in the master site, (d) position of the slave, (e) contact force in the slave site, and (f) feedback force from the slave site.



In this set of experiments, the laparoscopic impulse engine produced by Immersion Corporation, shown in Fig. 5.7, was used for the user to generate position commands and receive feedback reflection forces. The impulse engine is a 5 DOF joystick designed specifically for force reflection in the VR MIS (Minimally Invasive Surgery) simulation. Fig. 5.8 shows the experimental setup. The 3-D VR scene including a VR mobile manipulator (This manipulator was constructed by the advanced home robot research group in NCTU), was used for the experiment. When the human operator manipulated the laparoscopic impulse engine, the operation commands would be sent into the local site PC to generate position commands. Then, the local site PC displayed the predicted robot position in the 3-D VR scene on the monitor to provide real-time visual information and sent the position commands to the remote site via the Internet. The real-time predicted force reflection also generated by local site PC at the same time. Master site impedance controller was used to prevent too large force reflection from damaging the impulse engine. Another 3-D VR scene was located at the slave site to represent the actual slave robot and environment. When the remote PC receives delayed commands from the master site, it would display the controlled robot position on the slave site monitor and calculate the contact force. The Sliding-mode-impedance controller in the slave site was used to perform path tracking and force stability maintenance. We performed the same compliance task as that in the simulations and Internet experiments that moved remote virtual mobile manipulator to contact the virtual wall in 3-D VR scene between two computers in NCTU. The experimental results are shown in Fig. 5.9. Fig. 5.9(a) shows the master position commands generated from the local site PC according to the operation commands we applied on the impulse engine. Figs. 5.9(b)-(c) show the calculated predicted position and contact force of the remote slave system, respectively. The predicted force vibrated a little bit as shown in Fig. 5.9(c), mainly

due to the path resolution of the position commands. When we increased the commanded path resolution, the robot would move very slowly because the frame rate for the display of VR scene was around 60 to 70 Hz. Figs. 5.9(d)-(e) show the controlled slave position and force response in the VR scene according to the delay commands from the master. We found that the slave did follow the master, and the force response of the slave was very similar to the predicted force, as shown in Fig. 5.9(c). Fig. 5.9(f) shows the round-trip time delay measured during the experiments. From the experimental results, the system stability was achieved and the performance was satisfactory, in the presence of small experimental error, demonstrating the feasibility and effectiveness of the proposed bilateral control scheme.



Fig. 5.7 The laparoscopic impulse engine.

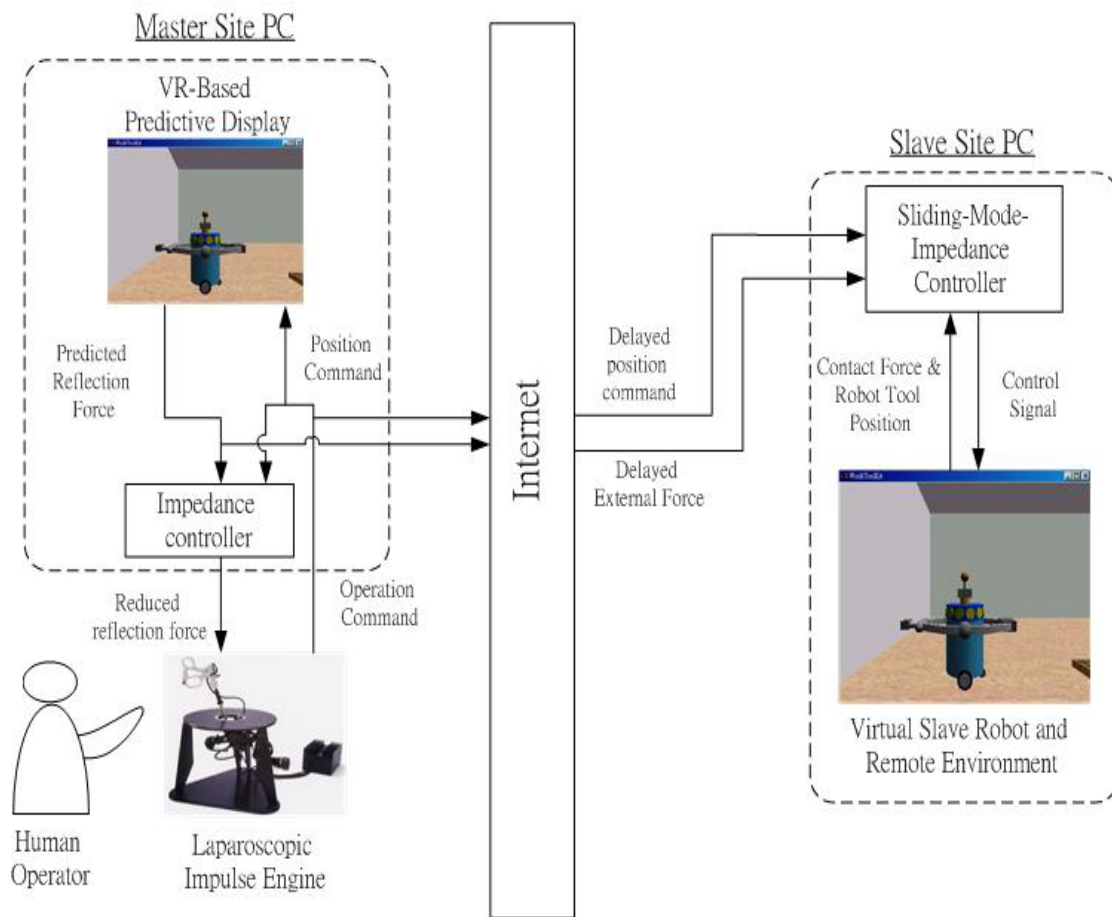


Fig. 5.8 The experimental setup.

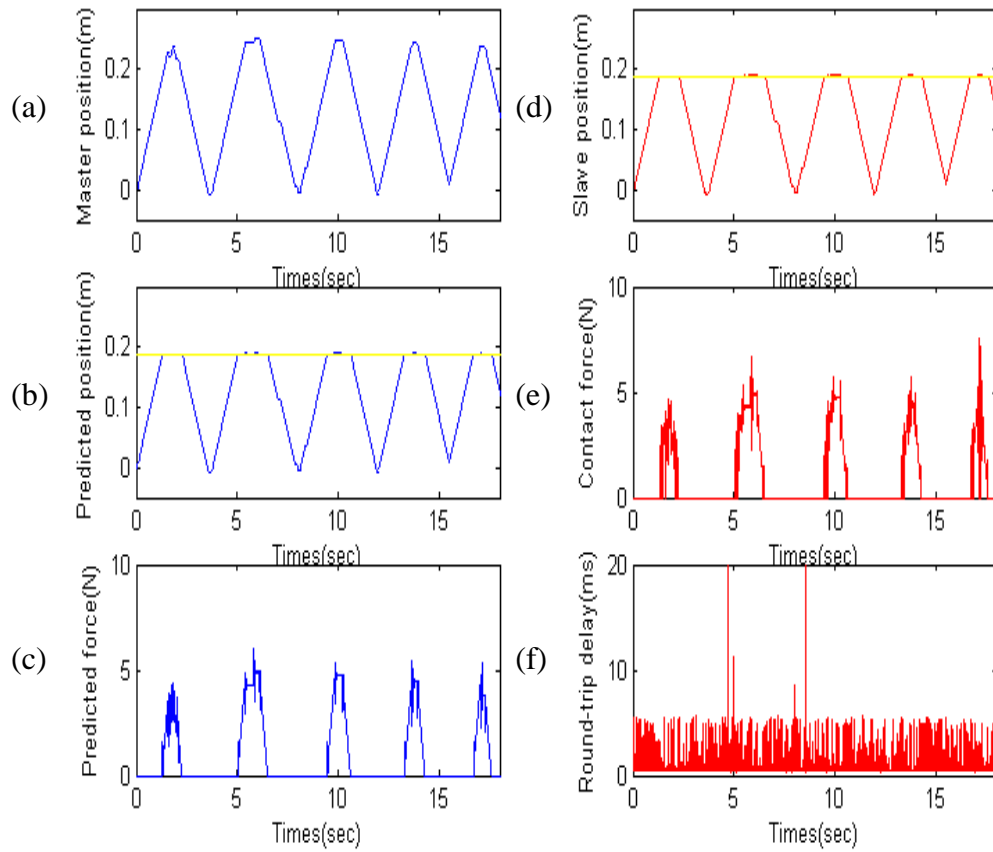



Fig. 5.9 Experimental results under the experimental setup as described in Fig. 5.8: (a) position of the master, (b) predicted position in the master site, (c) predicted virtual force in the master site, (d) position of the slave, (e) contact force in the slave site, and (f) the round-trip delay.

## Chapter 6

### Conclusion and Future work



In this thesis, we have developed a bilateral control scheme based on the sliding-mode-impedance controller for the networked VR-based telerobotic system. It is much simplified when compared with our previous work, thus making system stability and transparency analyses more meaningful. We then analyzed system transparency after system stability has been guaranteed. The system has preserved scaled environmental impedance within the bandwidth of human capability. We have also developed an event-synchronized teleoperation system for performance comparison. Simulation and experimental results have shown that the proposed scheme can achieve system stability under varying time delay. And, the system has exhibited much smoother motion and more natural force response when compared with the event-based system.

## 6.1 Future Work

To enhance this bilateral telerobotic system, some future works are suggested below:

1. The use of Internet to support the communications between the operator and the robot is quite attractive due to its worldwide availability for a telerobotic system, although time delay present in the network stands as the obstacle to achieve system synchronicity. Event-based control is a very popular method to eliminate the asynchronous phenomenon invoked by time delay. However, the event-based system exhibits unsmooth behavior and unnatural force response, which is not preferred in a telerobotic system. In our works, we have used the VR-based predictive display technique to provide predicted position and virtual contact force of the slave for the human operator in a real-time manner. However, the remote situation remains untackled. In others words, system synchronicity is still not achieved actually. As a future work, we will continue to develop a stable, transparent, and synchronous teleoperation system, which is certainly very challenging.
2. In this thesis, the experiments are basically performed in the simulated environment. In future, the physical system should be implemented to make the experimental results more convincing.
3. For real-time consideration, we should also develop more efficient network transmission method that is robust and fast in data transmission.

# Bibliography

- [1] N. Ando, J.-H. Lee, and H. Hashimoto, "A Study on Influence of Time Delay in Teleoperation," *IEEE/ASME International Conference on Advanced Intelligent Mechatronics*, pp. 317-322, 1999.
- [2] R. J. Anderson and M. W. Spong, "Bilateral Control of Teleoperators with Time Delay," *IEEE Trans. on Automation Control*, Vol. 34, No. 5, pp. 494-501, 1989.
- [3] R. J. Anderson and M. W. Spong, "Bilateral Control of Teleoperators with Time Delay," *IEEE Trans. on Robotics and Automation*, Vol. 13, No. 5, pp. 494-501, 1989.
- [4] D. Barney and T. Ken, "Distributed Robotics over the Internet," *IEEE Robotics & Automation Magazine*, Vol. 7, No. 5, pp. 22-27, 2000.
- [5] H. C. Cho, J. H. Park, K. Kim, and J. O. Park, "Sliding Mode-Based Impedance Controller for Bilateral Teleoperation under Varying Time-Delay," *IEEE Int. Conf. on Robotics and Automation*, pp. 1025-1030, 2001.
- [6] I. Elhajj, N. Xi, and Y. H. Liu, "Real-Time Control of Internet Based Teleoperation with Force Reflection," *IEEE Int. Conf. on Robotics and Automation*, pp. 3284-3289, 2000.
- [7] I. Elhajj, N. Xi, W. K. Fung, and Y. H. Liu, "Haptic Information in Internet-Based Teleoperation," *IEEE/ASME Trans. on Mechatronics*, Vol. 6, No. 3, pp. 295-303, 2001.
- [8] I. Elhajj, N. Xi, B. Song, M. M. Yu, W. T. Lo, and Y. H. Liu, "Transparency and Synchronization in Supermedia Enhanced Internet-Based Teleoperation," *IEEE Int. Conf. on Robotics and Automation*, pp. 2713-2718, 2002.
- [9] I. Elhajj, N. Xi, W. K. Fung, Y. H. Liu, Y. Hasegawa, and T. Fukuda, "Supermedia-Enhanced Internet-Based Telerobotics," *IEEE Trans. on Robotics and Automation*, Vol. 91, No. 3, pp. 396-421, 2003.
- [10] A. Goto, R. Inoue, T. Tezuka, and H. Yoshikawa, "A Research on Tele-operation Using Virtual Reality," *IEEE Int. Workshop on Robot and Human Communication*, pp. 147-152, 1995.
- [11] W. Gao, Y. Wang, and A. Homaifa, "Discrete-Time Variable Structure Control

- Systems”, *IEEE Transactions on Industrial*, vol. 42, No. 2, pp. 117-122, 1995.
- [12] K. Hirota and M. Hirose, “Providing Force Feedback in Virtual Environment,” *IEEE Computer Graphics and Applications*, Vol. 15, No. 5, pp. 22-30, 1995.
- [13] K. Kosuge, H. Murayama, and K. Takeo, “Bilateral Feedback Control of Telemanipulators via Computer Network,” *IEEE Int. Conf. on Robotics and Automation*, pp. 1380-1385, 1996.
- [14] K. Kosuge and H. Murayma, “Bilateral Feedback Control of Telemanipulator via Computer Network in Discrete Time Domain,” *IEEE Int. Conf. on Robotics and Automation*, pp. 2219-2224, 1997.
- [15] D. A. Lawrence, “Stability and Transparency in Bilateral Teleoperation,” *IEEE Trans. on Robotics and Automation*, Vol. 9, No. 5, pp. 624-637, 1993.
- [16] W. Leland, M. Taqqu, W. Willinger, and D. Wilson, “On the Self-Similar Nature of Ethernet Traffic,” *IEEE/ACM Trans. on Networking*, Vol. 2, No. 1, pp. 1-15, 1994.
- [17] Y. Liu, C. Chen, and M. Meng, “A Study on the Teleoperation of Robot Systems via WWW,” *IEEE Canadian Conference on Electrical and Computer Engineering*, pp. 836-840, 2000.
- [18] G. Niemeyer, J. Jacques, and E. Slotine, “Towards Force-Reflecting Teleoperation over the Internet,” *IEEE Int. Conf. on Robotics and Automation*, pp. 1909-1915, 1998.
- [19] R. Oboe and P. Fiorini, “A Design and Control Environment for Internet-Based Telerobotics,” *IEEE Int. J. Robotics Research*, Vol. 17, No. 2, pp. 433-449, 1998.
- [20] J. H. Park and H. C. Cho, “Sliding Mode Controller for Bilateral for Bilateral Teleoperation with Time Delay,” *IEEE/ASME Int. Conf. on Advanced Intelligent Mechatronics*, pp. 311-316, 1999.
- [21] J. H. Park and H. C. Cho, “Sliding Mode Control of Bilateral Teleoperation Systems with Force-Reflection on the Internet,” *IEEE/RSJ Int. Conf. on Intelligent Robots and Systems*, pp. 1187-1192, 2000.
- [22] L. F. Penin, K. Matsumoto, and S. Wakabayashi, “Force Reflection for Ground Control of Space Robots,” *IEEE Robotics & Automation Magazine*, Vol. 7, No. 4, pp. 50-63, 2000.
- [23] P. A. Prokopiou, S. G. Tzafestas, and W. S. Harwin, “Towards Variable Time Delays Robust Telemanipulation Through Master State Prediction,” *IEEE/ASME Int. Conf. on Advantaged Intelligent Mechatronics*, pp. 305-310, 1999.
- [24] R. Paul, “Problems and research issues associated with the hybrid control of force and displacement”, *IEEE Int. Conf. on Robotics and Automation*, pp. 1966-1971, 1987.



- [25] D. W. Repperger, C. A. Phillips, and T. L. Chelette, "A Study on Spatially Induced 'Virtual Force' with an information Theoretic Investigation of Human Performance," *IEEE Trans. on Systems, Man, and Cybernetics*, Vol. 25, No. 10, pp. 1392-1404, 1995.
- [26] A. Sulzmann and J. Jacot, "3D Computer Graphics Based Interface to Real Microscopic World for  $\mu$ -Robot Telemanipulation and Position Control," *IEEE Int. Conf. on Systems, Man, and Cybernetics*, pp. 286-291, 1995.
- [27] J. E. Speich, K. Fite, and M. Goldfarb, "A Method for Simultaneously Increasing Transparency and Stability Robustness in Bilateral Teleoperation," *IEEE Int. Conf. on Robotics and Automation*, pp.2671-2676, 2000.
- [28] T. J. Tarn, N. Xi, A. K. Bejczy, "Path-Based Approach to Integrated Planning and Control for Robotic Systems", *Automatica*, Vol. 32, No. 12, pp. 1675-1687, 1996.
- [29] N. Xi, "Event-Based Planning and Control for Robotic Systems," Doctoral Dissertation, Washington University, December 1993.
- [30] Y. Yokokohji, T. Imaida, and T. Yoshikawa, "Bilateral Teleoperation under Time-Varying Communication Delay," *IEEE Int. Conf. on Intelligent Robots and Systems*, pp. 1854-1859, 1999.
- [31] Y. Yokokohji, T. Teruhiro, and T. Yoshikawa, "Bilateral Control with Time-Varying Delay including Communication Blackout," *IEEE Int. Conf. on Haptic Interfaces for Virtual Environment and Teleoperator Systems*, pp. 285-292, 2002.
- [32] K. H. Zaad and S. E. Salcudean, "Transparency in Time-Delayed Systems and the Effect of Local Force Feedback for Transparent Teleoperation," *IEEE Trans. on Robotics and Automation*, Vol. 18, No. 1, pp. 108-114, 2002.
- [33] M. Zhu and S. E. Salcudean, "Achieving Transparency for Teleoperator System under Position and Rate Control," *IEEE Int. Conf. on Robotics and Automation*, pp. 7-12, 1995.
- [34] 陳永平, 可變結構控制設計, 全華科技圖書股份有限公司, 1999.
- [35] 黃俊堯, 黃耀文, 許景華, 陳孝忠, WinSock 網路程式設計之鑰, 資訊人文文化有限公司, 1996.
- [36] 施威銘研究室, Internet 協定 TCP/IP 觀念與實做, 旗標出版社, 2002.
- [37] 張智星, MATLAB 程式設計與應用, 清蔚科技, 2000.
- [38] 古頤榛, VISUAL C++ 6 教學範本, 碁峰資訊, 2000.